Science of the Total Environment 663 (2019) 852–866

Contents lists available at ScienceDirect

Science of the Total Environment

journal homepage: www.elsevier.com/locate/scitotenv

Mapping heat-related health risks of elderly citizens in mountainous area: A case study of Chongqing, China

Wei Zhang [a,b,*], Caigui Zheng [c,d], Feng Chen [e]

[a] School of Geographical Sciences, Southwest University, Chongqing 400715, China
[b] Research Center of Urban and Regional Planning in Southwest China, Chongqing 400715, China
[c] Chongqing Institute of Surveying and Planning for Land Resources and Housing, Chongqing 401121, China
[d] Chongqing Engineering Research Center for Land Use and Remote Sensing Monitoring, Chongqing 401121, China
[e] Zhejiang Institute of Meteorological Sciences, Hangzhou 310017, China

HIGHLIGHTS

- Mapping heat health risk of elderly population in a large mountainous area at a raster scale
- A new repeatable methodology was developed for mapping heat risk.
- This model can provide more targeted information to decision makers.
- This model improved the flexibility and comparability of heat risk assessment tool.
- This model is particularly valuable for quantifying heat risk in developing countries.

GRAPHICAL ABSTRACT

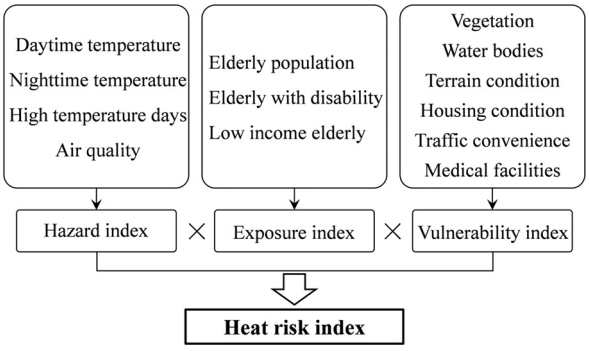

ARTICLE INFO

Article history:
Received 5 October 2018
Received in revised form 21 December 2018
Accepted 19 January 2019
Available online 22 January 2019

Editor: Wei Huang

Keywords:
Heat risk
Elderly population
Raster scale
Mountainous area
Developing countries
Chongqing

ABSTRACT

Heat wave becomes a leading cause of weather-related illness and death across the world under the background of climate change, urban heat island, and population ageing. Heat health risk assessment is an important starting point for heat-related morbidity and mortality reduction within the risk governance framework. Chongqing, a mountainous municipality with a fast rate of population ageing in China, was selected as a case study for mapping the heat health risk of the elderly population at a raster scale. The results indicated that the high heat hazard and human exposure areas were mainly distributed in the metropolitan areas, which largely resulted in high heat health risk in the urban areas. However, the high heat vulnerability pixels were mainly concentrated at the remote mountainous regions which have broken terrains and low socioeconomic statuses. Compared with traditional general heat risk indicator, this new model can provide more targeted spatial information to decision makers, and is helpful to improve the flexibility and comparability of heat risk assessment tool. Furthermore, this new model is particularly valuable for quantifying heat health risk in developing countries with limited open access data.

1. Introduction

Heat wave is a leading cause of weather-related illness and death across the world (Hu et al., 2017). In 2003, unprecedented heat waves in Western Europe resulted in approximately 70,000 excess deaths;

* Corresponding author at: School of Geographical Sciences, Southwest University, No.2 Tiansheng road, Beibei district, Chongqing, China.
E-mail address: zwei1997@swu.edu.cn (W. Zhang).

https://doi.org/10.1016/j.scitotenv.2019.01.240
0048-9697/

and the 2010 heat wave in Russia caused an estimated 55,000 deaths (Keller, 2013). In the United States of America, the 2006 heat wave in California resulted in 1200 additional hospitalizations and 16,000 additional emergency room visits (Pincetl et al., 2016). In Australia, heat waves are the most dangerous natural hazard over the past 200 years (Hatvanikovacs et al., 2016). Since 1800, over 4000 deaths have been attributed to heat waves in Australia, twice the number of deaths due to either flood or cyclones (Loughnan et al., 2014). In the summer of 2013, a total of 5758 heat-related illness cases were recorded by Chinese Center for Disease Control and Prevention (China CDC), about twice the numbers of 2011 and 2012 (Gu et al., 2016). To make matters worse, there is growing evidence that the intensity, frequency, and duration of heat waves are likely to escalate in the future because of climate change, urban heat island and population ageing (Meehl and Tebaldi, 2004; Mora et al., 2017). Therefore, as an important starting point for heat-related morbidity and mortality reduction within the risk governance framework, research on heat health risk assessment and mapping has increased rapidly in recent years (Krstic et al., 2017; Chen et al., 2018).

An increasing number of studies utilized Crichton's Risk Triangle as the conceptual framework of heat health risk assessment (Crichton, 1999; Buscail et al., 2012; Chen et al., 2018). According to this conceptual framework, the character and severity of heat waves not only depend on the heat waves, but also on the exposure and vulnerability. Therefore, the heat health risk is described as a function of hazard, exposure, and vulnerability (Tomlinson et al., 2011). Many previous studies assessed and mapped heat health risk based on this conceptual framework, and proofed that their results are reliable (Reid et al., 2012; Wolf et al., 2014). However, generally speaking, the heat health risk assessment tools are still in the early stages of development (Loughnan et al., 2014; Wolf et al., 2015), and many theoretical and methodological issues need to be further discussed. (1) Most previous studies utilized daytime temperature as the hazard index. The main data sources include air temperature data from field observations (Macnee and Tokai, 2016; Hu et al., 2017), and land surface temperature (LST) data that derived from satellite imagines (Weber et al., 2015; Luis et al., 2016). However, two indices are usually ignored in previous studies. The first one is the nighttime temperature. Previous studies have shown that if nighttime temperatures remain high, heat may accumulate in buildings (Givoni, 1998), and then lead to the increase of mortality during heat waves (Hoffmann et al., 2008; Son et al., 2012). The second one is air quality. The interactions of global climate change, urban heat islands, and air pollution are predicted to increase the health burdens of urban populations (Harlan and Ruddell, 2011), and there is growing evidence proofed the synergistic effect between high temperatures and air quality on mortality (Filleul et al., 2006; Willers et al., 2016). (2) Census data, which is usually counted with some specific statistical areas (e.g., postal code, census tract, zip code areas) and published by the government, is a fundamental component of heat risk assessment. So most previous studies on heat risk assessment were conducted at the census unit level (Johnson et al., 2012; Aubrecht and Özceylan, 2013; Heaton et al., 2014; Li et al., 2016). However, census data only provide the total population of each census unit and usually ignore the spatial heterogeneity of population within the border of each census unit (Loughnan et al., 2014; Bao et al., 2015). Because detailed spatial distribution information of population is important to assess casualties, determine the needs of rescue supplies, and properly implement evacuation plans during the disaster events (Aubrecht et al., 2013; Tenerelli et al., 2015), lacking of detailed spatial distribution information of population is a major shortcoming of census unit-based heat health risk assessment tools to decision-making and disaster relief (Ho et al., 2015). Therefore, it is important to develop an effective and low-cost model for estimating the spatial distribution of high heat-related risk population at a finer scale. (3) To date, most of the previous studies on heat risk (Johnson et al., 2009; Aubrecht and Özceylan, 2013) or heat vulnerability assessment (Chuang, 2012; Weber et al., 2015; Li et al., 2016; Macnee and Tokai, 2016) combined several different vulnerable groups (such as infants, the elderly, and people of low income) in their analysis to calculate a general heat risk indicator. However, this method usually leads to some problems. Firstly, the comparability among different assessment results is poor. Due to some reasons, such as data availability and the subjective preferences of researchers (Romero-Lankao et al., 2012), different studies usually select different heat vulnerable groups, resulting in poor comparability among different studies. For example, Dong et al. (2014) selected only two vulnerable groups, while Johnson et al. (2012) selected 14 vulnerable groups. Secondly, it's unable to provide effective guidelines to decision makers. Generally speaking, different vulnerable groups need different resources and aids during heat waves (Mees et al., 2014). For instance, infants and elderly people need additional ambulance facilities and health care workers because they have poor physical resistance to heat (Xu et al., 2014; Benmarhnia et al., 2017); language barriers need more multi-language heat information and guidelines; while the most needed support for low income people is free public 'cool spot', such as well shaded park, water body, and library (Sampson et al., 2013; Zografos et al., 2016). However, traditional general heat risk indicator couldn't provide that useful information.

Up to date, most of the heat health risk assessment studies were conducted in developed countries and mainly focused on cities (Zhu et al., 2014; Morabito et al., 2015; Aminipouri et al., 2016; Pincetl et al., 2016). However, due to inadequate public health infrastructure (Balogun et al., 2010), lower health risk perception (Tao et al., 2013) and socioeconomic status (Neuman et al., 2013; Priyanka and Chakravarty, 2015), population in rural areas and developing countries may be more vulnerable to heat waves than urban areas and developed countries (Sheridan and Dolney, 2003; Wu et al., 2011; Henderson et al., 2013). China is a developing country with the largest elderly population in the world and one of the fastest rates of population ageing in human history (Li and Zhang, 2015). The proportion of elderly people (aged 60 years and over) in China is expected to increase from about 10.0% in 2000 to 35% in 2050 (Lutz et al., 2008), which means the number of elderly people in China will be about 500 million in 2050. Lower socioeconomic status, rapidly increasing for ageing population and the inadequacy of healthcare expenditures (Nie, 2016) highlight the health risk of the elderly population in China. The purpose of this interdisciplinary study is to assess and map heat-related health risks of elderly citizens at a raster scale through Crichton's risk triangle conceptual framework. Chongqing, one of the largest inland mountainous cities (Hu et al., 2016) and the most famous summer "oven" in China (Li et al., 2017), was selected as a case study for mapping heat-related health risks of elderly citizens. In this study, the research questions addressed are as follows: 1) How to assess the heat-related health risks of a specific vulnerable group with limited open data in developing countries? 2) How to improve the accuracy and comparability of heat-related health risks assessment tool? 3) What is the spatial pattern of heat-related health risks of elderly people in a large, mountainous area?

2. Material and methods

2.1. Study area

Chongqing (28°10′–32°13′N, 105°11′–110°11′E), with a total area of 82,370 km^2, is the youngest municipality of China (Zhang and Deng, 2010). It is situated in the middle and lower reaches of the Yangtze River in the sub-tropical climate zone. By the end of 2016, the total population of Chongqing reached 33.9 million, and 64% of the population lives in urban areas. Chongqing is famous for the towering mountains, roaring rivers, and hot summer. It constitutes a complex terrain, with

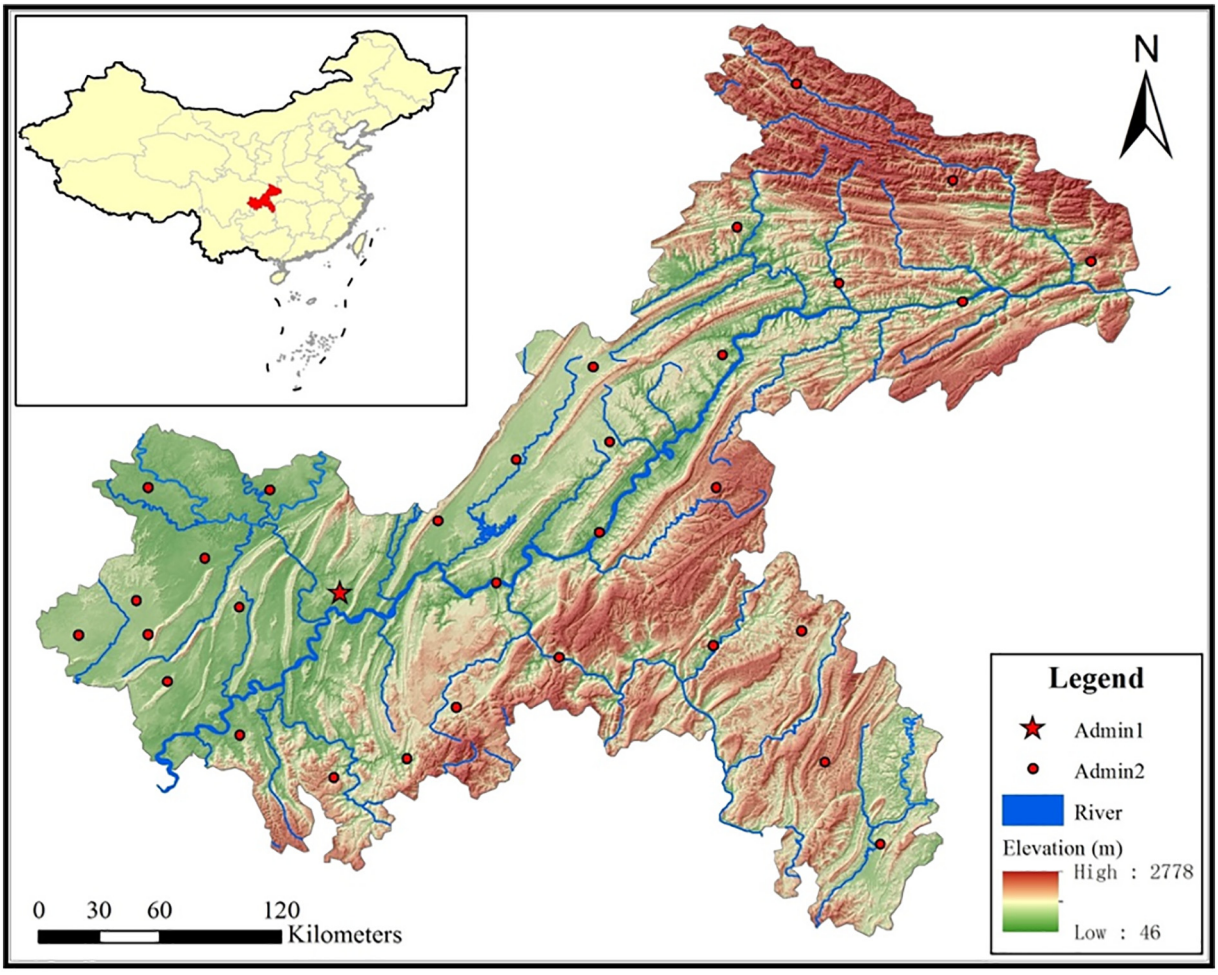

Fig. 1. Study area location, elevation, hydrographic net, and administrative centers. (a) Data source of elevation: Advanced Spaceborne Thermal Emission and Reflection Radiometer (ASTER) Global Digital Elevation Model (GDEM) V002, which was obtained from the website of National Aeronautics and Space Administration (NASA). Hillshade was used for 3D effect. (b) Data source of hydrographic net and administrative centers: National catalogue service for geographic information in China. (c) "Admin 1" in the legend represents the capital of Chongqing, it includes 9 districts; while "Admin 2" represents the administrative centers of other counties and districts of Chongqing.

hills and mountains accounting for 76% of the total area (Fig. 1). The climate of Chongqing belongs to humid subtropical climate (Cwa) according to Köppen climate classification (Peel et al., 2007), which characterized by hot and humid summers. Chongqing is known as one of China's "four ovens", with the average temperature of summer (June to August) ranging from 26 to 29 °C. Due to climate change and rapid urbanization (Zhou et al., 2010), the number of extremely high temperature days (daily maximum temperature exceeds 35 °C) in Chongqing is rising (Fig. 2).

2.2. Data collection and preprocessing

(1) Land surface temperature (LST) data

Two Moderate Resolution Imaging Spectroradiometer (MODIS) LST products, MOD11A1 (daytime) and MYD11A1 (nighttime), were used in this study. All the LST products were downloaded from the website of The Level-1 and Atmosphere Archive & Distribution System (LAADS) Distributed Active Archive Center (DAAC), National Aeronautics and Space Administration (NASA), with the spatial resolution of 1 km (NASA, 2010a). The daytime and nighttime LST data from three exceptional hot days was selected: Jul. 2, 2010; Aug. 11, 2010 and Aug. 12, 2010; and the daily maximum air temperature for those 3 days is 38 °C, 40.6 °C and 40.2 °C respectively. At last, the 3-day average LST data was used in this study. The MODIS Reprojection Tool (MRT) 4.1 was used for the mosaicking, reprojection, and resampling of all the LST products.

(2) Extremely high temperature days

Extremely high temperature days at the county level for Chongqing during 2012 to 2017 were obtained from Chongqing Climate Bulletin 2012–2017 published by Chongqing Meteorological Bureau. The definition of extremely high temperature day is the day when the daily maximum temperature exceeds 35 °C according to the China Meteorological Administration (Dong et al., 2014).

(3) Air quality data

Excellent and good air quality days at the county level for Chongqing from 2014 to 2017 were obtained from Ecological and Environmental Monitoring Center of Chongqing. Air quality is divided into 6 levels in China based on Technical Regulation on Ambient Air Quality Index (on trial) (HJ 633-2012) published by Ministry of Environmental Protection of China, which are excellent (level 1), good (level 2), mild pollution (level 3), medium pollution (level 4), heavy pollution (level 5) and severe pollution (level 6). More details about AQI were presented in Appendix A.

(4) Census data

Census data at the county level for Chongqing (40 counties in total) were obtained from China's Sixth (2010) National Census, which is the

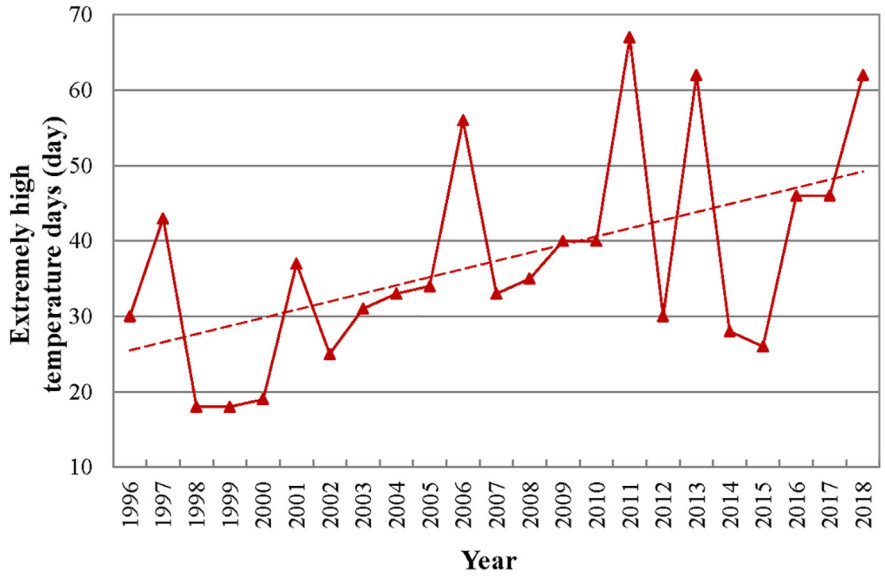

Fig. 2. The temporal trend of the extremely high temperature days in Chongqing. (a) The extremely high temperature days refers to the days when the daily maximum temperature exceeds 35 °C according to China Meteorological Administration; (b) data source: National Meteorological Information center in China.

latest nationwide census of China. The following five indexes were derived from census data: total elderly population (60+); elderly people with disability; elderly people with low income; dwellings without bathing facilities; dwellings built before 1980.

(5) Statistical data

The density of highways (km/km^2) and total beds of health institutions for the year 2010 at the county level for Chongqing (40 counties in total) were obtained from Chongqing Statistical Yearbook 2011.

(6) Vegetation data

Enhanced Vegetation Index (EVI) data (MOD13Q1) for the year of 2010 was downloaded from the website of LAADS DAAC, NASA, with the spatial resolution of 250 m (NASA, 2010b). MRT 4.1 software was used for preprocessing. In order to eliminate cloud contamination and other noises, maximum value compositing (MVC) was employed to generate a new EVI composite data (EVI_{max}) based on multi-temporal EVI data (Zhu et al., 2013). For match other datasets, cubic resampling technique provided by ArcGIS 10.0 was used for resampling EVI data to the spatial resolution of 1 km.

(7) Digital elevation model (DEM) data

The Advanced Spaceborne Thermal Emission and Reflection Radiometer (ASTER) Global Digital Elevation Model (GDEM) V002 dataset used in this study was obtained from the website of NASA (NASA, 2011). The spatial resolution of original GDEM data is 30 m. Slope tool in ArcGIS 10.0 was used to generate the slope data at a 30 m raster scale. The relief degree of land surface (RDLS) at a 30 m raster scale was calculated by the following formula (Hu and Si, 2014):

$$R = H_{max} - H_{min} \quad (1)$$

where R is the RDLS of a specific raster; H_{max} is the maximum elevation within a 7 × 7 neighborhood around it, and H_{min} is the minimum elevation within the same 7 × 7 neighborhood. Focal Statistics and Raster Calculator tools in ArcGIS 10.0 were used for calculations.

Finally, in order to match other datasets, cubic resampling technique provided by ArcGIS 10.0 was used for resampling elevation data, slope data and RDLS data to the spatial resolution of 1 km.

(8) Water bodies data

Global Surface Water data used in this study was obtained from the website of the United States Geological Survey (USGS) (USGS, 2012). This dataset is a classification of persistent surface water bodies during the 2000 to 2012 interval at a 30 m spatial resolution. Persistent surface water was assigned to pixels that were classified as water over 50% of the time from candidate 2000 to 2012 growing season observations, not including cloud and shadow-affected data. This surface water dataset was resampled at 1 km spatial resolution by the same cubic resampling technique, which is consistent with other datasets.

(9) Nighttime Lights (NTL) Imagery

Defense Meteorological Satellite Program Operational Linescan System (DMSP/OLS) Nighttime Lights (NTL) data (Version 4) used in this study was obtained from the website of the National Geophysical Data Center of the National Oceanic and Atmospheric Administration (NOAA) with a 30″ spatial resolution (NOAA, 2010). The stable NTL data in the year 2010 for Chongqing was resampled to a 1 km spatial resolution by cubic resampling technique in ArcGIS 10.0 to match other datasets.

(10) Hospital visits data

Monthly total hospital visits data in the summer period (June to August) at the county level for Chongqing during 2015 to 2017 was obtained from Monthly Statistics on Health and Family Planning in Chongqing that published by Health and Family Planning Commission of Chongqing (HFPCC) (HFPCC, 2018).

2.3. Methodology

2.3.1. Conceptual framework of heat risk assessment

Crichton's Risk Triangle (Crichton, 1999; Morabito et al., 2015) was employed as the conceptual framework of heat health risk assessment for the elderly population in this research. In this framework, the character and severity of heat waves not only depend on the heat waves, but also on the exposure and vulnerability. Therefore, heat health risk is described as a function of hazard, exposure, and vulnerability (Tomlinson et al., 2011). (1) Heat hazard. In the context of heat health risk assessment, heat hazard is usually recognized as the increase

in daily temperature (Ho et al., 2015; Luis et al., 2016; Krstic et al., 2017), which could be historical, measured, or predicted (Chen et al., 2018). With the developing of heat-related researches, many studies are beginning to pay attention to the effects of nighttime temperature (Amaya et al., 2017; Obradovich et al., 2017), heat wave durations (Unal et al., 2013) and air quality (Merbitz et al., 2012; Ikram et al., 2015; Willers et al., 2016) on public health, and noticed the synergistic effect among heat waves, air quality and urban environment on morbidity and mortality (Ho et al., 2017). Therefore, four indicators were selected to construct a heat hazard index: daytime temperature, nighttime temperature, extremely high temperature days, and air quality. (2) Human exposure. The exposure represents what is exposed to the hazard (Tomlinson et al., 2011). For heat health risk assessment, where there are no people, there is no exposure, and consequently, no risk (Buscail et al., 2012). Therefore, population density and its spatial distribution were usually used to estimate the exposure (Dugord et al., 2014; Hu et al., 2017). In this study, three indicators derived from census data at the county level were selected to construct a human exposure index for elderly people: total elderly population, elderly with disability, and elderly with low income. An elevation-adjusted human settlement index (EAHSI) integrated by multisource data (Hu et al., 2017; Chen et al., 2018) was used to disaggregate and map the spatial distribution of the census data for the elderly population at 1 km resolution. (3) Heat vulnerability. Heat vulnerability is the propensity to be adversely affected because the disadvantages of the physical environment, social resources and the characteristics of a specific group influence their capacity to cope with, mitigate, and recover from heat waves (Buscail et al., 2012; Hu et al., 2017). In this study, four natural condition indicators at 1 km resolution (vegetation, water bodies, slope, and the relief degree of land surface), and four social condition indicators at the county level (dwellings without bathing facilities, dwellings built before 1980, density of highways, and total beds of health institutions) were selected to construct a heat vulnerability index.

The final heat risk index (HRI) for elderly population was produced by the multiplication of three normalized indices (heat hazard index, human exposure index, and heat vulnerability index) with equal weights, because no standard conclusion exists from which a more appropriate weighting among each index can be derived (Johnson et al., 2012; Ho et al., 2015; Chen et al., 2018).

2.3.2. Heat hazard

Four indicators were employed to estimate the heat hazard of Chongqing. The first two indicators are daytime and nighttime temperature derived from MOD11A1 and MYD11A1 products with a spatial resolution of 1 km. The MODIS series LST data has many advantages to estimate heat hazard in a large area for its wide spatial coverage, including both day and night measurement, and high thermal accuracy. For MODIS LST data is a reliable tool to capture the complex urban-rural gradient of surface temperature, an increasing number of studies utilized it to estimate heat hazard (Morabito et al., 2015; Weber et al., 2015; Chen et al., 2018). In this study, both daytime and nighttime LST data were averaged by 3 MODIS LST products during three exceptional hot days to eliminate cloud contamination and other noises. The third indicator is extremely high temperature days at the county level from 2012 to 2017. The definition of extremely high temperature day is the day when the daily maximum temperature exceeds 35 °C according to the China Meteorological Administration (Dong et al., 2014). More high temperature days usually indicate a higher heat load of senior citizens, and consequently, higher risk (Vandentorren et al., 2006; Fink et al., 2017). The fourth indicator is excellent and good air quality days at the county level from 2014 to 2017. There is growing evidence that interactions between high temperatures and air pollution produced a synergistic effect on human health and contributed to higher heat risk (Shaposhnikov et al., 2014). All four hazard indicators were normalized by the z-score method to scale each indicator to a mean of 0 and a standard deviation of 1(Zhang et al., 2014).

Pearson correlation and collinearity diagnostics tool in SPSS software were utilized to examine the relationships among four indicators and eliminate the redundant information. At last, we aggregated those indicators and then normalized it to obtain the heat hazard index ranging from 0 to 100 in the study area by ArcGIS 10.0.

2.3.3. Human exposure

Many literatures show that the adverse effects of heat waves on health can be more serious for elderly persons than other groups due to their fragile physical condition (Conti et al., 2006; Foroni et al., 2007; Urban et al., 2017). In addition, people with disability (Pincetl et al., 2016; Macintyre et al., 2017) and low income population (Li et al., 2016; Zografos et al., 2016) are two widely accepted fragile groups during heat waves. So it is quite clear that the heat health risks for elderly people with disability and low income will be rising exponentially during heat waves. In this study, three indicators were selected to estimate the exposure of elderly people (≥60) in Chongqing: total elderly population, elderly with disability, and elderly with low income.

Pearson correlation and principle component analysis (PCA) were performed by SPSS software to reduce the dimension and eliminate the redundant information among indicators (Jiao and Guo, 2014). One combined principal component has been extracted to represent the human exposure index at the county level.

The DMSP/OLS Nighttime Lights (NTL) data is a powerful tool to monitor the nighttime lights associated with human activities, so it was widely used as a valuable covariate to estimate population density and distribution at a raster scale across the world (H. Ma et al., 2014; L. Ma et al., 2014; Savory et al., 2017; Tan et al., 2018). Elevation-adjusted human settlement index (EAHSI) integrated by stable NTL images, DEM data, and EVI data is highly correlated with population distribution and greatly reduced the saturation effect in DMSP/OLS data, so the application of this method is increasing (Yang et al., 2013; H. Ma et al., 2014; L. Ma et al., 2014; Hu et al., 2017). In this study, EAHSI was used to disaggregate and map the spatial distribution of human exposure index at 1 km resolution. The formulas are as follow:

$$\mathrm{EAHSI} = \frac{(1-\mathrm{EVI}_{max}) + OLS_{\mathrm{nor}}}{(1-OLS_{\mathrm{nor}}) + \mathrm{EVI}_{max} + OLS_{\mathrm{nor}} \times \mathrm{EVI}_{max}} \times DEM^{-0.341} \times P_{elder} \quad (2)$$

$$\mathrm{OLS_{nor}} = (\mathrm{OLS} - \mathrm{OLS_{min}})/(\mathrm{OLS_{max}} - \mathrm{OLS_{min}}) \quad (3)$$

where $\mathrm{EVI_{max}}$ is the maximum value of EVI data for the year of 2010; DEM is the elevation of each raster; $\mathrm{P_{elder}}$ is the percentage of the elderly population for each county/district; $\mathrm{OLS_{nor}}$ is the normalized value of the stable NTL image; $\mathrm{OLS_{max}}$ and $\mathrm{OLS_{min}}$ are the maximum and minimum value of NTL image.

Finally, we normalized the human exposure index ranging from 0 to 100 by ArcGIS 10.0 at a 1 km raster scale.

2.3.4. Heat vulnerability

Multiple inhabitation environment factors and socioeconomic indicators have been demonstrated to affect the relation between heat wave and health outcomes in previous studies (Reid et al., 2012; Son et al., 2012; Bélanger et al., 2016; Tapia et al., 2017). Eight indicators were employed to construct a heat vulnerability index of Chongqing based on literature review and data availability. (1) Vegetation and water bodies have been widely reported for its heat stress mitigation function by cooling its surrounding areas in hot days (Bencheikh and Rchid, 2012; Battista et al., 2016; Zhang et al., 2016), so proximity to vegetation and water bodies were selected as two vulnerability indicators based on the Enhanced Vegetation Index (EVI) data and Global Surface Water data with the spatial resolution of 1 km. Firstly, the focal statistics tool was used to calculate for each pixel location a statistic of vegetation/surface water pixels within a 3 × 3 circle neighborhood around it. A bigger output value of a pixel means more vegetation/

surface water pixels around it and has a higher capacity to relieve heat stress. Secondly, the z-score method was used to normalize above two vulnerability indicators to a mean of 0 and a standard deviation of 1. At last, we obtained the maps of above two vulnerability indicators with the spatial resolution of 1 km. (2) Terrain condition. Chongqing is the largest mountainous city in China (Li et al., 2018). The mountainous terrain is an important factor for the fragile ecological environment and poverty in Chongqing (Liu et al., 2014), and has caused inaccessibility, inconvenience, and unavailability of timely medical services (Raza et al., 2017). Therefore, slope and the relief degree of land surface were selected as two vulnerability indicators based on DEM data. A bigger value of slope or the relief degree of land surface for one pixel means a lower capacity to relieve heat stress. The z-score method was used to normalize above two indicators. At last, we obtained the maps of two terrain condition indicators with the spatial resolution of 1 km. (3) Housing condition. Housing conditions, such as housing type, structure, and cooling equipment, are associated with heat-related mortality and morbidity during heat waves (Tomlinson et al., 2011; Palmer et al., 2014; Macintyre et al., 2017). So we selected "dwellings without bathing facilities", and "dwellings built before 1980" at the county level as two vulnerability indicators based on census data of Chongqing. Those two indicators were normalized by the z-score method and mapped at the county level. (4) Traffic convenience. Traffic condition is an important factor for vulnerability groups to seek cooling place or medical services timely on a hot summer day (Aminipouri et al., 2016). In this research, the density of highways (km/km^2) at the county level for Chongqing was selected as a vulnerability indicator. We normalized this indicator by the z-score method and mapped it at the county level. (5) Medical facilities. Accessibility to medical services is important for elderly persons to recover from heat stress (Luis et al., 2016), so we selected total beds of health institutions at the county level as a vulnerability indicator. We normalized this indicator by the z-score method and mapped it at the county level.

Pearson correlation and collinearity diagnostics tool from SPSS software were utilized to examine the relation and eliminate the redundant information among eight indicators. At last, we aggregated those indicators and then normalized it to obtain the heat vulnerability index ranging from 0 to 100 in the study area by ArcGIS 10.0.

3. Results

3.1. Heat hazard

As is shown in Fig. 3a and b, the spatial patterns of daytime and nighttime temperature were similar, and both of them present a strong urban heat island (UHI) effects. The hotspots of daytime and nighttime temperature were mainly distributed in the metropolitan area in the west, while the temperature of the northeast and southeast mountainous regions is much lower due to their high vegetation coverage.

The spatial pattern of extremely high temperature days for Chongqing is presented in Fig. 3c. The areas with longer duration of high temperature days were mainly distributed in the northeast of Chongqing,

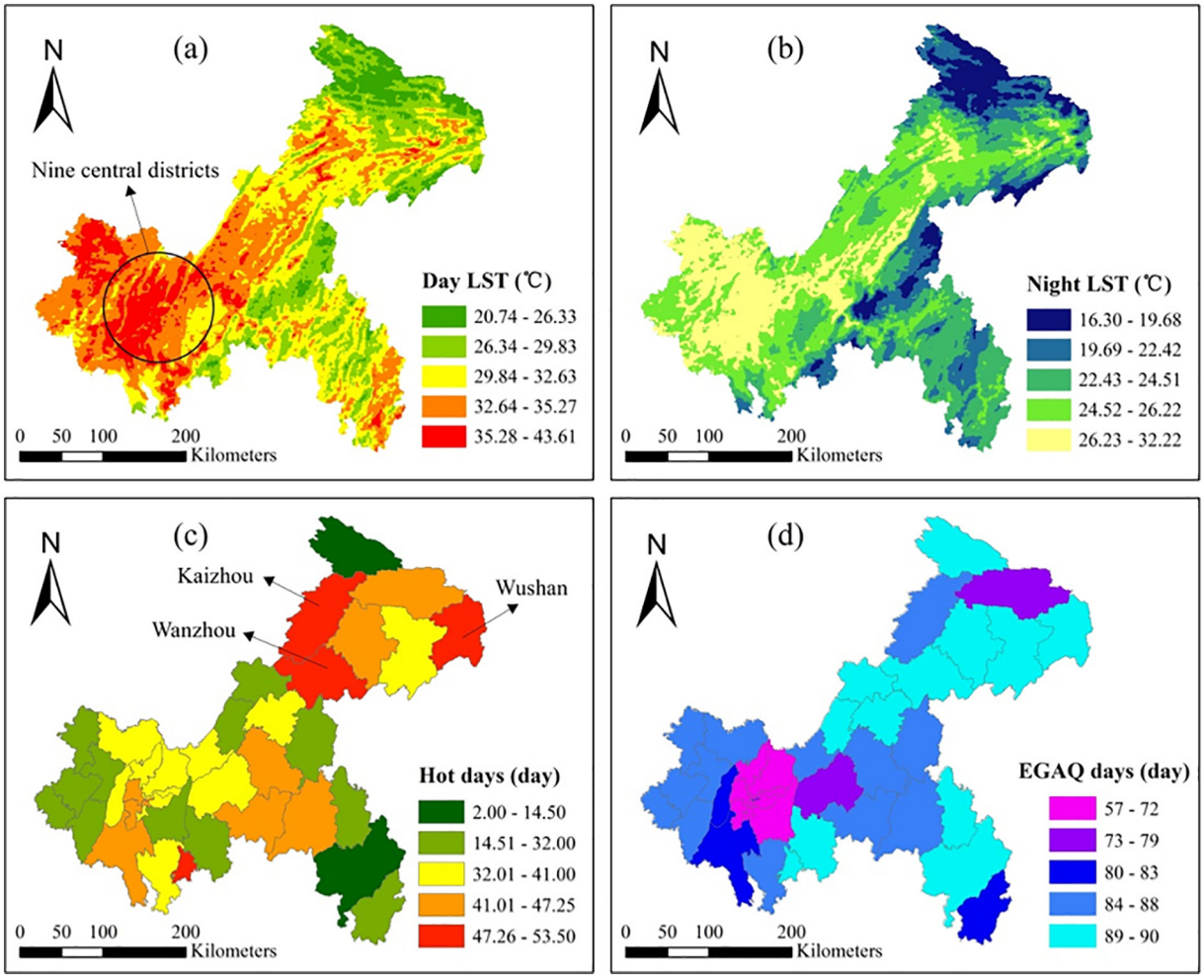

Fig. 3. The spatial distribution of the four hazard indicators in Chongqing. (a). Daytime Land surface temperature (LST); (b) nighttime LST; (c) extremely high temperature days per year; (d) excellent and good air quality days per summer. The summer period includes June, July and August in Chongqing.

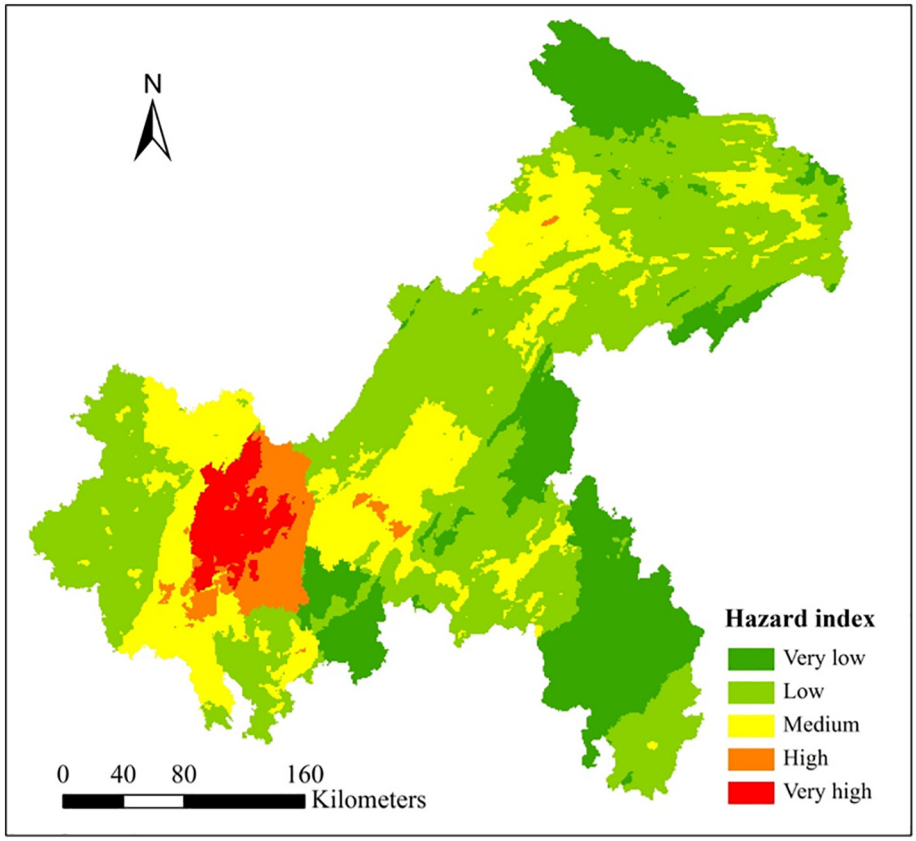

Fig. 4. The spatial distribution of the heat hazard index for Chongqing.

narrow section of Yangtze River valley (Fig. 1), such as Kaizhou district, Wanzhou district, and Wushan county. The strong foehn warming effect is the main reason for its long duration of extremely high temperature days in this area (Speirs et al., 2010; H. Ma et al., 2014; L. Ma et al., 2014). The spatial pattern of high temperature days is quite different with the LST data presented in Fig. 3a and b. LST data is transient (perhaps a few seconds) temperature data at a wide spatial scale; while "high temperature days" data is long-term (summer period) statistics data at a point (meteorological station). Therefore, although the high temperature areas of remote counties are limited, it is possible that some remote counties have more high temperature days than metropolitan areas.

Fig. 3d presented the excellent and good air quality days for Chongqing. As is shown in Fig. 3d, nine central districts of Chongqing have the minimum number (<72 days per summer) of excellent and good air quality days, which means a worse air quality. Chongqing is one of most important manufacturing center in China, and its major industries include the automotive industry, electronic information industry, chemical industry, energy industry, etc. which inevitably lead to a certain degree of environmental pollution. In addition, most of the industries are concentrated at the nine central districts of Chongqing. In 2010, nine central districts contributed 38.45% Gross Domestic Product (GDP) for the secondary industry with just 6.64% of total land area. Therefore, the rapid development of secondary industry is the main reason for the poor air quality of the nine central districts in Chongqing.

The results of Pearson correlation and collinearity diagnostics tool in SPSS indicated that the Pearson correlation coefficient of daytime and nighttime temperature at the county level is 0.971 (p-value < 0.001), and the tolerance values in collinearity Statistics are 0.050 and 0.051 respectively, which means that there is collinearity between these two indicators. Therefore, we simply averaged those two indicators into a combined indicator named surface temperature. We examined the indicators again and found that there is no collinearity among three indicators (surface temperature, extremely high temperature days, and excellent and good air quality days), so we aggregated those three indicators and then normalized it to obtain the heat hazard index ranging from 0 to 100 in the study area by ArcGIS 10.0. Fig. 4 presented the spatial distribution of heat hazard index for Chongqing. As is shown in Fig. 4, the highly-affected area is the metropolitan area, which has a strong UHI effect and more serious environmental pollution.

3.2. Human exposure

The results of Pearson correlation indicated all the Pearson correlation coefficients among three exposure indicators are higher than 0.890 (p-value < 0.001), so principle component analysis (PCA) was performed by SPSS software to reduce the dimension and eliminate the redundant information among indicators (Jiao and Guo, 2014). One combined principal component is generated from three indicators by the variance weighted approach (Luis et al., 2016), which means that the percentages of three variances explained by this component were used as the weights for aggregating (Macnee and Tokai, 2016). After all, the human exposure index at the county level was calculated by the following formula:

$$HEI = 0.993 \times P_{elder} + 0.986 \times D_{elder} + 0.958 \times L_{elder} \quad (4)$$

where HEI is human exposure index; P_{elder} is the total elderly population aged 60 years and over; D_{elder} is the elderly population with disability; L_{elder} is the elderly population with low income.

EAHSI was used to disaggregate and map the human exposure index at a raster scale. As is shown in Fig. 5, the EAHSI is highly correlated with population distribution, which means EAHSI is a good proxy to estimate

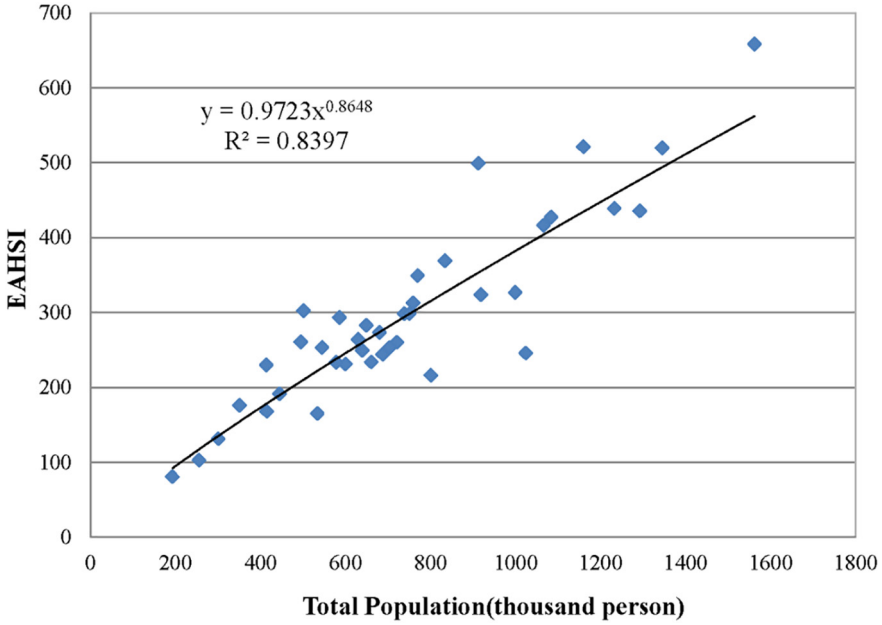

Fig. 5. The scatterplots of the total population and accumulated EAHSI value for counties/districts of Chongqing.

the spatial delineation of human exposure index in Chongqing (Chen et al., 2018). The spatial pattern of human exposure index for Chongqing (Fig. 6) indicated that high human exposure pixels were mainly concentrated at big cities like nine central districts and Wanzhou district. In fact, the above ten districts have gathered 31.27% of the total population in Chongqing with just 10.82% land area.

3.3. Heat vulnerability

The results of Pearson correlation and collinearity diagnostics indicated that the Pearson correlation coefficient of "slope" and "the relief degree of land surface" at the county level is 0.997 (p-value < 0.001); while the correlation coefficient of "dwellings without bathing facilities"

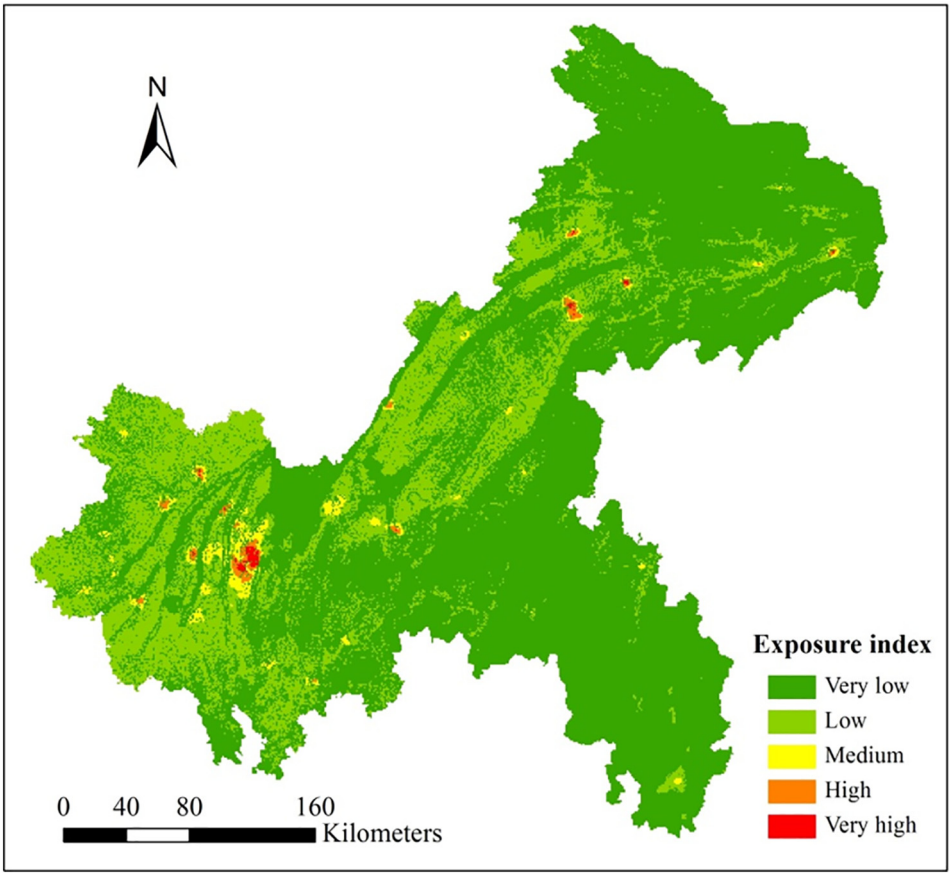

Fig. 6. The spatial pattern of the human exposure index for Chongqing.

Table 1
Pearson correlation coefficients of vulnerability indicators.

Indicators	X1	X2	X3	X4	X5	X6	X7	X8
X1	1.000							
X2	−0.544**	1.000						
X3	0.810**	−0.355*	1.000					
X4	0.812**	−0.332*	0.997**	1.000				
X5	−0.355*	0.823**	−0.212	−0.185	1.000			
X6	−0.451**	0.834**	−0.316 *	−0.289	0.983**	1.000		
X7	−0.568**	0.457**	−0.491**	−0.470**	0.366*	0.420**	1.000	
X8	−0.249	0.746**	−0.228	−0.206	0.895**	0.869**	0.382*	1.000

Notes: (1) X1: Proximity to vegetation; X2: Proximity to water bodies; X3: Slope; X4: Relief degree of land surface; X5: Dwellings built before 1980; X6: Dwellings without bathing facilities; X7: Density of highways; X8: Total beds of health institutions. (2) * means correlation is significant at the 0.05 level (2-tailed); ** means correlation is significant at the 0.01 level (2-tailed). (3) SPSS software was used for data processing.

and "dwellings built before 1980" at the county level is 0.983 (p-value < 0.001) (Table 1). Collinearity diagnostic results also indicated that there is collinearity among some indicators (Table 2). Therefore, we averaged "slope" and "the relief degree of land surface" into a combined indicator named terrain condition, and generated another combined indicator named dwelling condition based on "dwellings without bathing facilities" and "dwellings built before 1980". We examined the indicators again and found that there is no collinearity among six indicators (proximity to vegetation, proximity to water bodies, terrain condition, dwelling condition, density of highways, and total beds of health institutions) (Table 2), so we aggregated those six indicators and then normalized it to obtain the heat vulnerability index ranging from 0 to 100 in the study area by ArcGIS 10.0.

As is shown in Fig. 7, high heat vulnerability pixels were mainly concentrated at the northeast and southeast mountainous regions, such as Wushan and Wuxi counties in the northeast, and Youyang Xiushan, Pengshui counties in the southeast. Those counties have rich vegetation, while with broken terrains and low socioeconomic statuses, which lead to worse medical services, traffic condition and housing condition. In 2010, those five counties have gathered 8.78% of the total population in Chongqing with 22.45% land area and contributed only 3.64% Gross Domestic Product (GDP) for Chongqing.

3.4. Heat risk

As is shown in Fig. 8, the high heat risk areas were mainly distributed in the metropolitan area and other densely populated areas of Chongqing, including the nine central districts of Chongqing, Wanzhou, Hechuan, Kaizhou, and Yunyang. Low heat risk areas were mainly distributed in the remote mountainous area, such as Chengkou, Wuxi in the northeast, and Youyang Qianjiang, Pengshui counties in the southeast. Generally, the spatial pattern of heat risk index (HRI) was driven by the distribution of heat hazard and human exposure.

3.5. Validation

Validation is an important component for mapping heat risk (Reid et al., 2012; Li et al., 2016). In this study, monthly hospital visits in the summer period (June to August) at the county level (n = 40) for Chongqing were available. Therefore, we calculated the accumulated HRI of each county by means of zonal statistic tool in ArcGIS 10.0. The results indicated that the Pearson correlation coefficients between HRI and summer hospital visits is 0.873 (p-value < 0.001) at the county level, which shows a good fit of the heat risk assessment model presented in this study. In addition, polynomial regression was employed to predict summer hospital visits using the accumulated HRI as the independent variable. As is shown in Fig. 9, the estimated summer hospital visits correlated very well with the spatial variations in accumulated HRI ($R^2 = 0.924$).

4. Discussion

To the best of our knowledge, this is the first heat health risk map for the elderly population in China, and the first heat health risk map for the elderly population at the pixel level and regional scale in the world. Elderly population has been of primary concern in many previous researches (Morabito et al., 2015; Chien et al., 2016; Benmarhnia et al., 2017; Hu et al., 2017) for their higher mortality risk and hospital admission rate for respiratory and other heat-related diseases on hot days (Kosatsky et al., 2012; Aminipouri et al., 2016). At a time of most people can expect to live into their 60s and beyond, it is a certain trend that the population ageing is rapidly accelerating worldwide (Dey, 2017). The global ageing population (people aged 60 years and over) is expected to increase from 605 million in 2000 to 2 billion in 2050, which means that the proportion of ageing population will double from 11% to 22% over the same period (Kanasi et al., 2016). Spatial heat risk assessment is not just an important tool to find out the spatial distribution of high temperature area and locate the fragile groups most vulnerable to heat, but also a valuable method for conducting spatially explicit heat health warning and future heat health risk projection (Hu et al., 2017).

Most previous studies focused on developed countries and urban areas (Wolf and Mcgregor, 2013; Hu et al., 2017; Voelkel et al., 2018), but the heat-related risk of fragile groups located in developing countries and rural areas is of equal importance to the former one. Take the elderly population as an example, although the trend of population ageing was

Table 2
Collinearity Statistics results of vulnerability indicators.

Indicators before processing	Tolerance	VIF	Indicators after processing	Tolerance	VIF
Proximity to vegetation	0.164	6.080	Proximity to vegetation	0.187	5.338
Proximity to water bodies	0.233	4.296	Proximity to water bodies	0.238	4.207
Slope	0.005	215.916	Terrain condition	0.279	3.588
Relief degree of land surface	0.004	224.186	Dwelling condition	0.131	7.629
Density of highways	0.540	1.852	Density of highways	0.606	1.649
Total beds of health institutions	0.138	7.234	Total beds of health institutions	0.156	6.417
Dwellings built before 1980	0.016	61.539			
Dwellings without bathing facilities	0.019	53.532			

Notes: (1) VIF is Variance inflation factor. (2) SPSS software was used for data processing.

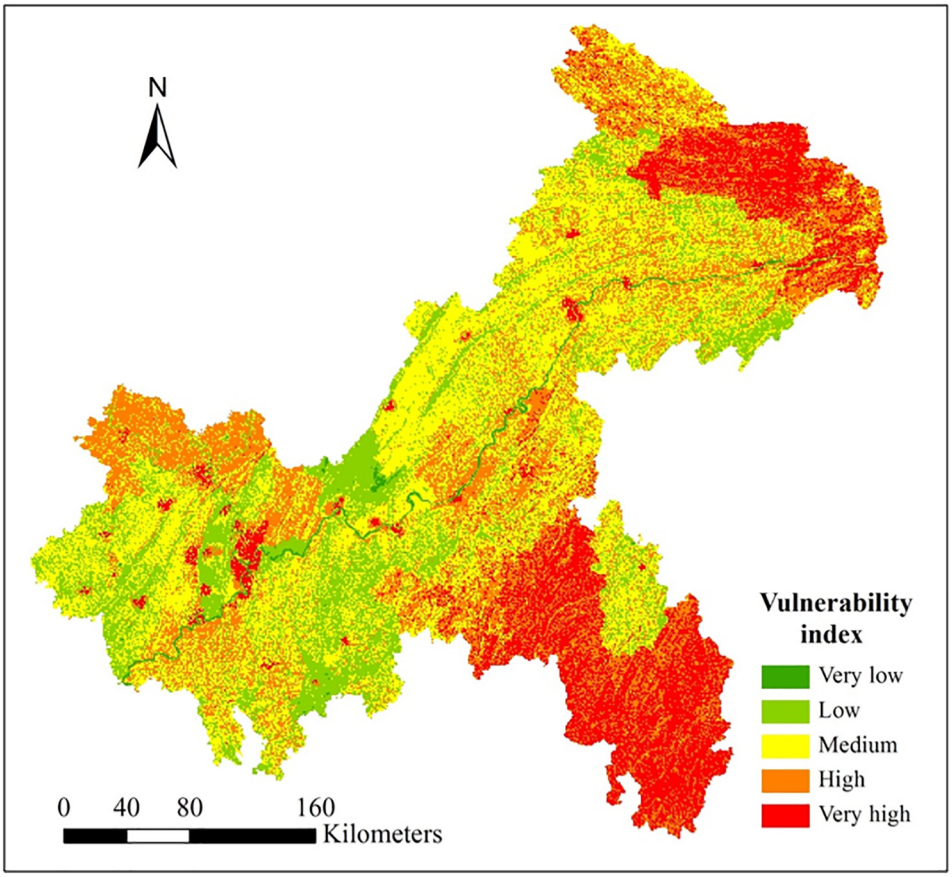

Fig. 7. The spatial pattern of the heat vulnerability index for Chongqing.

started in high-income countries like Japan and Italy, it is now low- and middle-income countries that are experiencing the fastest population ageing. Projections from the World Health Organization (WHO) indicated that the 80% of elderly people will live in low- and middle-income countries like China and Brazil in 2050 (WHO, 2018). In many developing countries, globalization and global connectivity make it easier for younger generations to migrate to urban areas; while elderly family members were left in poor rural areas without enough support (Abas et al., 2009). In China, more elderly people are expected to live in rural areas than in large megacities. Projections from Cai and Wang (2005) indicated that the proportion of elderly people (people aged 60 years and over) in rural and urban areas by 2030 will be 21.8% and 14.8%, respectively. Compared with urban population, the rural population has lower socioeconomic status, less medical resources, lower health risk perception to heat waves and seldom employed adaptation behaviors during extreme heat events (Tao et al., 2013), especially in low- and middle-income countries (WHO, 2015). This study provided a new method for the future heat risk or heat vulnerability assessment: replacing the traditional general heat risk indicator with individual heat risk indicator links to one specific fragile group. In this way, not only more targeted spatial information is provided to decision makers, but also is helpful to improve the flexibility and comparability of heat risk assessment tools. The reasons are as follows: (1) The traditional heat risk assessment usually combined several different fragile groups into a general heat risk indicator, so we need to renew the whole model and map the heat risk again if the data of new fragile groups becomes available. However, the mapping results of different fragile groups are independent in the new model presented in this study, so it's unnecessary to modify the previous mapping results if we need to map the heat risk of some new fragile groups. Therefore, the flexibility and extensibility of heat risk assessment tool will be enhanced. (2) Lacking comparable data and results is still a challenge for researches on heat risk and heat vulnerability assessment (Lissner et al., 2012). Because the information of fragile groups is usually derived from census data released by local governments, and the statistical standards and contents are non-uniform among different countries and regions, so different studies usually contained different fragile groups, leading to poor comparability among heat risk assessment results. However, the comparability of different studies will be greatly enhanced in the framework of this new model because it maps the heat-related risk for one specific fragile group each time.

This study built a new heat risk indicator to map heat health risk in mountainous regions. Considering the synergistic effect among heat waves, air quality and urban environment on morbidity and mortality (Filleul et al., 2006; Willers et al., 2016; Ho et al., 2017), we employed more indexes to build a new heat hazard indicator, which include daytime LST, nighttime LST, extremely high temperature days per year, excellent and good air quality days per summer. As is shown in Fig. 3, the spatial patterns of high temperature days (Fig. 3c) and air quality (Fig. 3d) are quite different with daytime and nighttime LST (Fig. 3a and b), which means those newly employed indexes have a significant impact on heat hazard indicator. We selected three indexes to estimate the human exposure indicator: total elderly population, elderly with disability, and elderly with low income; and then an Elevation-adjusted human settlement index (EAHSI) (Yang et al., 2013; Hu et al., 2017) was used to disaggregate and map the spatial pattern of human exposure index at a raster scale. As far as we know, this is the first raster-based human exposure map for elderly people. We employed some terrain indexes to build a new heat vulnerability indicator on account of Chongqing is a large region with many hills and mountains. The mountainous terrain is an important factor for the fragile ecological environment and poverty in developing countries (Liu et al., 2014), and

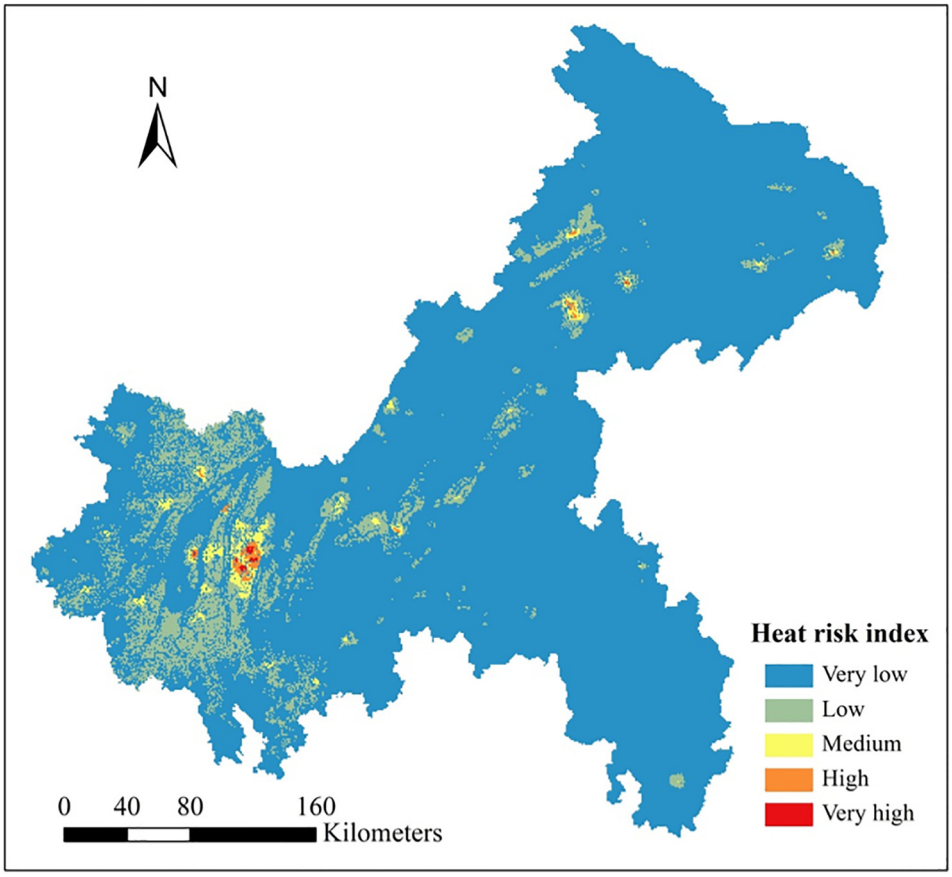

Fig. 8. The spatial pattern of the heat risk index for the elderly population in Chongqing.

has caused inaccessibility, inconvenience, and unavailability of timely medical services (Raza et al., 2017). However, previous studies seldom employed terrain indexes as heat vulnerability indicators; so this study provides a reference for the selection of heat vulnerability indicators in mountainous regions. The validation results (Fig. 9) indicated that the new heat risk indicator presented in this study performs well for heat risk assessment.

Our results indicated that the high hazard areas were mainly distributed in the metropolitan area (Fig. 4), which has a strong UHI effect and more serious environmental pollution. This result is consistent with the studies by Chen et al. (2018) and Hu et al. (2017). The high human exposure areas of Chongqing were mainly concentrated at big cities like nine central districts and Wanzhou district (Fig. 6) for those areas concentrated a large number of elderly people. This result is consistent with the study by Hu et al. (2017) which conducted in Zhejiang province, China; because both of Chongqing and Zhejiang are mountainous areas with similar spatial patterns on population distribution. However, our result on human exposure is contradicts with the study by Tomlinson et al. (2011) which conducted in Birmingham, UK. The possible reason is that Birmingham is located in the plain area of a developed country, and many people prefer to live in suburbs. In this study, the high heat vulnerability areas were mainly distributed at the remote rural regions (Fig. 7). This result is contradicts with the study by Aubrecht and Özceylan (2013) which showed high heat vulnerability areas are mainly located in the urbanized areas of the U.S. National Capital Region, but agree with previous studies by Hu et al. (2017), Henderson et al. (2013) and Wu et al. (2011) who suggested that rural population may be more vulnerable to heat wave than urban ones. Furthermore, our results indicated that the spatial pattern of heat risk was generally consistent with the heat hazard layer and human exposure layer, which means hazard and exposure are the main driving factors that contributed to potential high heat risk areas.

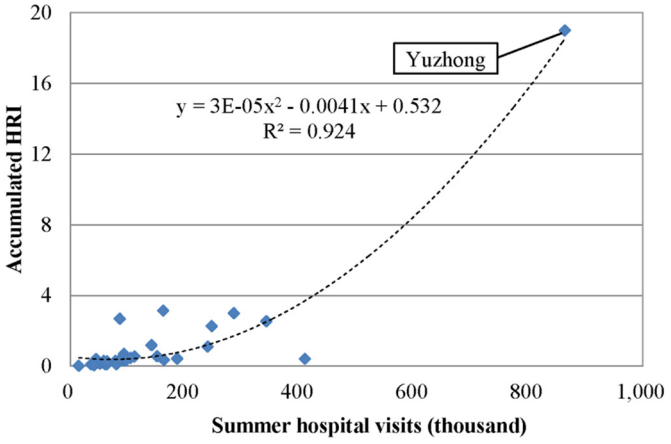

Fig. 9. Scatter diagram of the accumulated HRI and summer hospital visits at the county level for Chongqing. Yuzhong district is the political, economic and cultural center of Chongqing, and the Chongqing Municipal Government is located in this district.

This research is particularly valuable for quantifying heat health risk in developing countries. The reasons are as follows: (1) Lacking an established policy covering access to various environmental data and social survey data is an important obstacle for scientific progress and development in developing countries (Lang, 2011; Tomusange et al., 2017). This research employed a lot of open access data, such as MODIS LST products, MODIS vegetation products, Digital elevation model (DEM) data, DMSP/OLS Nighttime Lights (NTL) data and Global Surface Water data; so it offers a repeatable methodology that can be

utilized in many developing countries with limited opportunities for data sharing. (2) The basic spatial units of publicly released census data in developing countries are usually much larger than in developed countries. Therefore, the spatial differentiation information provided by census unit-based heat risk assessment in developing countries is much less than in developed countries. For example, the latest census data of China's Sixth National Census was published on Tabulation on the 2010 Population Census of the People's Republic of China by County, and the average area of basic spatial units (county/district) is 3354.48 km^2. While as for the latest census data of Australia (2016) released online, the average area of basic spatial units (Statistical Areas Level 1, SA1) is only 133.65 km^2 (Australian Bureau of Statistics, 2016). Furthermore, this gap is even larger at a city scale. The average area of district in Beijing is 1025.66 km^2, while the average area of SA1 in the Greater Sydney is 1.92 km^2 (Australian Bureau of Statistics, 2016). In order to match spatial units employed by the census, census unit-based heat risk assessment usually uses some spatial statistic methods like zoning or scaling for data processing (Bao et al., 2015; Ho et al., 2015), which inevitably lead to the modifiable areal unit problem (MAUP) and statistical bias (Ho et al., 2015; Schuurman et al., 2007). Obviously, the MAUP and statistical bias are more serious in developing countries than developed countries for its much larger basic spatial unit. Therefore, the raster-based heat risk assessment model presented in this study is more valuable for developing countries.

Despite its assets, there are still some limitations in this study. (1) Heat health risk assessment requires a wide variety of detailed data, while limited indexes were employed in this study due to data availability. For example, as for the hazard analysis, except for the factors already utilized in this study, other meteorological and environmental factors like humidity, wind speed (Johnson et al., 2009; Romero-Lankao et al., 2012) and urban dry island effect (Wang et al., 2012) are contribute to the impact of heat waves on public health too. In addition, the previous study indicated that people with pre-existing medical conditions are particularly vulnerable to heat waves (Romero-Lankao et al., 2012). However, this important human exposure index was not available in our research. The synergies between high temperature and the above factors should be further considered in future heat risk assessment. (2) Raster-based demographic and socioeconomic indicators are essential for heat vulnerability analysis. An Elevation-adjusted human settlement index (EAHSI) integrated by stable NTL images, DEM data, and EVI data used in this study partially solved this problem, but it also has some limitations. Firstly, the accuracy of EAHSI for population estimation still need to be further improved (Song et al., 2015; Hu et al., 2017). For example, EAHSI may attribute excessive population to industrial zones with sparkling nighttime light. Open street map data (Rosina et al., 2016), cloud computing services (Patel et al., 2015), geo-located tweets data (Patel et al., 2017) are useful tools to improve the accuracy of population mapping. Secondly, nighttime lights imagery-based EAHSI is suitable to estimate the spatial distribution of population at night, but has some deficiencies in mapping the daily distribution of the population. Considering that human exposure to heat wave is time-dependent (Hu et al., 2017), and population distribution varies widely from nighttime to daytime, especially in metropolitan areas, so the population distribution estimated by EAHSI introduced a degree of uncertainty in this study. For the commonly used census data do not capture the population dynamics as functions of space and time, so how to enhance the temporal resolution of population distribution becomes a great challenge in future heat risk assessment. Some new data sources like Subway Smart Card Data (Ma et al., 2017), mobile phone data (Deville et al., 2014) provide some unprecedented solutions for recording population distribution information with high temporal resolution. Finally, raster-based datasets for some socio-economic indicators like housing conditions, traffic conditions and medical facilities are still not available for the study area, so the spatial mismatch between those socio-economic indicators and other risk elements still exist in this research. (3) This study utilized multiple data sources with different collection dates. Such as 2010 daytime and nighttime LST data, 2010 census data, 2012–2017 high temperature days data, 2014–2017 air quality data and 2010 nighttime lights data. We admit that the discrepancy among different data sources inevitably created some temporal ambiguity during the modeling process. (4) Because detailed local health and mortality records for the elderly population were not available, so total hospital visits data in the summer period was utilized for validation in this research. Obviously, all-cause hospital visits data is not the best choice for validation here, and it inevitably has a certain impact on the accuracy of validation results.

5. Conclusions

This study presents a methodology for mapping the heat health risk of the elderly population in Chongqing, China at a raster scale. The results indicated that the high heat hazard and human exposure areas were mainly distributed in the metropolitan areas, which largely resulted in high heat health risk in the urban areas. However, the high heat vulnerability pixels were mainly concentrated at the remote mountainous regions that have broken terrains and low socioeconomic statuses. Our findings can provide the preliminary information for decision-makers. That information is useful for the government to prepare more targeted adaptation strategies and emergency planning for the elderly population and preventing heat stress for elderly people in Chongqing.

Compared with traditional general heat risk indicator, this new model can provide more targeted spatial information to decision makers, and is helpful to improve the flexibility and comparability of heat risk assessment tool. Furthermore, this new model is particularly valuable for quantifying heat health risk in developing countries with limited open access data.

Funding

This work was supported by Social Science Planning Project of Chongqing, China [grant number 2018PY57]; Fundamental Research Funds for the Central Universities [grant number SWU115003]; National Natural Science Foundation of China [grant number 41101039].

Acknowledgements

The authors acknowledge gratefully the advice by professor Phil McManus at the University of Sydney for his help in designing this research work. Additionally, gratitude is expressed to Elizabeth Duncan at the University of Sydney for her helps in data collection.

Appendix A. The calculation of the Air Quality Index (AQI)

According to Technical Regulation on Ambient Air Quality Index (on trial) (HJ 633-2012) published by the Ministry of Environmental Protection of China, AQI was calculated by the following formula:

$$AQI = max\{IAQI_1, IAQI_2, IAQI_3, \ldots, IAQI_n\} \quad (A.1)$$

where IAQI represents the Individual Air Quality Index of each pollutant, n is the number of pollutants. At present, six Individual Air Quality Indexes were measured: SO_2, NO_2, PM_{10}, $PM_{2.5}$, O_3, and CO.

Individual Air Quality Index (IAQI) was calculated by the following formula:

$$IAQI_i = \frac{IAQI_{Hi} - IAQI_{Li}}{BP_{Hi} - BP_{Li}}(C_i - BP_{Li}) + IAQI_{Li} \quad (A.2)$$

where $IAQI_i$ represents the IAQI of the i-th pollutant. C_i is the concentration of the i-th pollutant. BP_{Hi} and BP_{Li} are the high and low values of the pollutant concentration limit closest to C_i. $IAQI_{Hi}$ and $IAQI_{Li}$ are

the individual air quality indices corresponding to BP_{Hi} and BP_{Li}. The values of $IAQI_{Hi}$, $IAQI_{Li}$, BP_{Hi}, BP_{Li} were presented in Table A.1.

Table A.1
Threshold values of Individual Air Quality Index (IAQI) and pollutants.

IAQI	SO_2 ($\mu g/m^3$)	NO_2 ($\mu g/m^3$)	PM_{10} ($\mu g/m^3$)	CO (mg/m^3)	O_3 ($\mu g/m^3$)	$PM_{2.5}$ ($\mu g/m^3$)
0	0	0	0	0	0	0
50	50	40	50	2	100	35
100	150	80	150	4	160	75
150	475	18	250	14	215	115
200	800	280	350	24	265	150
300	1600	565	420	36	800	250
400	2100	750	500	48	>800	350
500	2620	940	600	60	>800	500

Notes: (1) data source: Technical Regulation on Ambient Air Quality Index (on trial) (HJ 633-2012). (2) The threshold values of SO_2, NO_2, PM_{10}, $PM_{2.5}$, and CO are the average value of 24 h, while the threshold values of O_3 is the average value of 8 h.

The threshold values and classification of AQI were presented in Table A.2.

Table A.2
The threshold values and classification of Air Quality Index (AQI) in China.

AQI	Level	Description
<50	I	Excellent
51–100	II	Good
101–150	III	Mild pollution
151–200	IV	Medium pollution
201–300	V	Heavy pollution
>300	VI	Severe pollution

Data source: Technical Regulation on Ambient Air Quality Index (on trial) (HJ 633-2012).

References

Abas, M.A., Punpuing, S., Jirapramukpitak, T., Guest, P., Tangchonlatip, K., Leese, M., Prince, M., 2009. Rural-urban migration and depression in ageing family members left behind. Br. J. Psychiatry 195, 54–60. https://doi.org/10.1192/bjp.bp.108.056143.

Amaya, M., Mohamed, M.T., Pingitore, N., Aldouri, R., Benedict, B., 2017. Community exposure to nighttime heat in a desert urban setting, El Paso, Texas. Int. J. Adv. Remote Sens. GIS 5, 1507–1513. https://doi.org/10.23953/cloud.ijarsg.42.

Aminipouri, M., Knudby, A., Ho, H.C., 2016. Using multiple disparate data sources to map heat vulnerability: Vancouver case study. Can. Geogr. 60, 356–368. https://doi.org/10.1111/cag.12282.

Aubrecht, C., Özceylan, D., 2013. Identification of heat risk patterns in the U.S. National Capital Region by integrating heat stress and related vulnerability. Environ. Int. 56, 65–77. https://doi.org/10.1016/j.envint.2013.03.005.

Aubrecht, C., Özceylan, D., Steinnocher, K., Freire, S., 2013. Multi-level geospatial modeling of human exposure patterns and vulnerability indicators. Nat. Hazards 68, 147–163. https://doi.org/10.1007/s11069-012-0389-9.

Australian Bureau of Statistics, 2016. 2016 census. http://www.abs.gov.au/websitedbs/censushome.nsf/home/about?opendocument&navpos=100, Accessed date: September 2019.

Balogun, A.A., Balogun, I.A., Adeyewa, Z.D., 2010. Comparisons of urban and rural heat stress conditions in a hot-humid tropical city. Glob. Health Action 3, 62. https://doi.org/10.3402/gha.v3i0.5614.

Bao, J., Li, X., Yu, C., 2015. The construction and validation of the heat vulnerability index, a review. Int. J. Environ. Res. Public Health 12, 7220–7234. https://doi.org/10.3390/ijerph120707220.

Battista, G., Carnielo, E., Vollaro, R.D.L., 2016. Thermal impact of a redeveloped area on localized urban microclimate: a case study in Rome. Energy Build. 133, 446–454. https://doi.org/10.1016/j.enbuild.2016.10.004.

Bélanger, D., Abdous, B., Valois, P., Gosselin, P., Sidi, E.A.L., 2016. A multilevel analysis to explain self-reported adverse health effects and adaptation to urban heat: a cross-sectional survey in the deprived areas of 9 Canadian cities. BMC Public Health 16, 1–11. https://doi.org/10.1186/s12889-016-2749-y.

Bencheikh, H., Rchid, A., 2012. The effects of green spaces (Palme trees) on the microclimate in Arides zones, case study: Ghardaia, Algeria. Energy Procedia 18, 10–20. https://doi.org/10.1016/j.egypro.2012.05.013.

Benmarhnia, T., Kihal-Talantikite, W., Ragettli, M.S., Deguen, S., 2017. Small-area spatiotemporal analysis of heatwave impacts on elderly mortality in Paris: a cluster analysis approach. Sci. Total Environ. 592, 288. https://doi.org/10.1016/j.scitotenv.2017.03.102.

Buscail, C., Upegui, E., Viel, J.F., 2012. Mapping heatwave health risk at the community level for public health action. Int. J. Health Geogr. 11, 1–9. https://doi.org/10.1186/1476-072X-11-38.

Cai, F., Wang, D., 2005. Demographic transition: implications for growth. In: Garnaut, R., Song, L. (Eds.), The China Boom and its Discontents. Asia Pacific Press, Canberra, pp. 34–52.

Chen, Q., Ding, M., Yang, X., Hu, K., Qi, J., 2018. Spatially explicit assessment of heat health risk by using multi-sensor remote sensing images and socioeconomic data in Yangtze River Delta, China. Int. J. Health Geogr. 17, 15. https://doi.org/10.1186/s12942-018-0135-y.

Chien, L.C., Guo, Y., Zhang, K., 2016. Spatiotemporal analysis of heat and heat wave effects on elderly mortality in Texas, 2006–2011. Sci. Total Environ. 562, 845–851. https://doi.org/10.1016/j.scitotenv.2016.04.042.

Chuang, W.C., 2012. Vulnerability to extreme heat in Metropolitan Phoenix: spatial, temporal, and demographic dimensions. Prof. Geogr. 64, 286–302. https://doi.org/10.1080/00330124.2011.600225.

Conti, S., Masocco, M., Meli, P., Minelli, G., Palummeri, E., Solimini, R., Toccaceli, V., Vichi, M., 2006. General and specific mortality among the elderly during the 2003 heat wave in Genoa (Italy). Environ. Res. 103, 267–274. https://doi.org/10.1016/j.envres.2006.06.003.

Crichton, D., 1999. The Risk Triangle. Tudor Rose, London.

Deville, P., Linard, C., Martin, S., Gilbert, M., Stevens, F.R., Gaughan, A.E., Blondel, V.D., Tatem, A.J., 2014. Dynamic population mapping using mobile phone data. Proc. Natl. Acad. Sci. U. S. A. 111, 15888. https://doi.org/10.1073/pnas.1408439111.

Dey, A.B., 2017. World report on ageing and health. Indian J. Med. Res. 145, 150–151. https://doi.org/10.4103/0971-5916.207249.

Dong, W., Liu, Z., Zhang, L., Tang, Q., Liao, H., Li, X., 2014. Assessing heat health risk for sustainability in Beijing's Urban Heat Island. Sustainability 6, 7334–7357. https://doi.org/10.3390/su6107334.

Dugord, P.A., Lauf, S., Schuster, C., Kleinschmit, B., 2014. Land use patterns, temperature distribution, and potential heat stress risk – the case study Berlin, Germany. Comput. Environ. Urban. Syst. 48, 86–98. https://doi.org/10.1016/j.compenvurbsys.2014.07.005.

Filleul, L., Cassadou, S., Médina, S., Fabres, P., Lefranc, A., Eilstein, D., Le, T.A., Pascal, L., Chardon, B., Blanchard, M., 2006. The relation between temperature, ozone, and mortality in nine French cities during the heat wave of 2003. Environ. Health Perspect. 114, 1344–1347. https://doi.org/10.1289/ehp.8328.

Fink, R., Eržen, I., Medved, S., 2017. Symptomatic response of the elderly with cardiovascular disease during the heat wave in Slovenia. Cent. Eur. J. Public Health 25, 260–266. https://doi.org/10.21101/cejph.a4496.

Foroni, M., Salvioli, G., Rielli, R., Goldoni, C.A., Orlandi, G., Zauli, S.S., Guerzoni, A., Maccaferri, C., Daya, G., Mussi, C., 2007. A retrospective study on heat-related mortality in an elderly population during the 2003 heat wave in Modena, Italy: the Argento Project. J. Gerontol. A Biol. Sci. Med. Sci. 62, 647–651. https://doi.org/10.1093/gerona/62.6.647.

Givoni, B., 1998. Effectiveness of mass and night ventilation in lowering the indoor daytime temperatures. Part I: 1993 experimental periods. Energy Build. 28, 25–32. https://doi.org/10.1016/S0378-7788(97)00056-X.

Gu, S., Huang, C., Li, B., Chu, C., Liu, Q., 2016. Heat-related illness in China, summer of 2013. Int. J. Biometeorol. 60, 131–137. https://doi.org/10.1007/s00484-015-1011-0.

Harlan, S.L., Ruddell, D.M., 2011. Climate change and health in cities: impacts of heat and air pollution and potential co-benefits from mitigation and adaptation. Curr. Opin. Environ. Sustain. 3, 126–134. https://doi.org/10.1016/j.cosust.2011.01.001.

Hatvanikovacs, G., Belusko, M., Skinner, N., Pockett, J., Boland, J., 2016. Drivers and barriers to heat stress resilience. Sci. Total Environ. 571, 603–614. https://doi.org/10.1016/j.scitotenv.2016.07.028.

Heaton, M.J., Sain, S.R., Greasby, T.A., Uejio, C.K., Hayden, M.H., Monaghan, A.J., Boehnert, J., Sampson, K., Banerjee, D., Nepal, V., 2014. Characterizing urban vulnerability to heat stress using a spatially varying coefficient model. Spat. Spatiotemporal Epidemiol. 8, 23–33. https://doi.org/10.1016/j.sste.2014.01.002.

Henderson, S.B., Wan, V., Kosatsky, T., 2013. Differences in heat-related mortality across four ecological regions with diverse urban, rural, and remote populations in British Columbia, Canada. Health Place 23, 48–53. https://doi.org/10.1016/j.healthplace.2013.04.005.

HFPCC, 2018. Monthly statistics on health and family planning in Chongqing. http://www.cqwsjsw.gov.cn/Html/1/tjsj/, Accessed date: June 2019.

Ho, H.C., Knudby, A., Huang, W., 2015. A spatial framework to map heat health risks at multiple scales. Int. J. Environ. Res. Public Health 12, 16110–16123. https://doi.org/10.3390/ijerph121215046.

Ho, H.C., Wong, M.S., Yang, L., Shi, W., Yang, J., Bilal, M., Chan, T.C., 2017. Spatiotemporal influence of temperature, air quality, and urban environment on cause-specific mortality during hazy days. Environ. Int. 112, 10–22. https://doi.org/10.1016/j.envint.2017.12.001.

Hoffmann, B., Hertel, S., Boes, T., 2008. Increased cause-specific mortality associated with 2003 heat wave in Essen, Germany. J. Toxic. Environ. Health A 71, 759. https://doi.org/10.1080/15287390801985539.

Hu, W., Si, B.C., 2014. Revealing the relative influence of soil and topographic properties on soil water content distribution at the watershed scale in two sites. J. Hydrol. 516, 107–118. https://doi.org/10.1016/j.jhydrol.2013.10.002.

Hu, Y., Yin, Z., Ma, J., Du, W., Liu, D., Sun, L., 2016. Energy-related GHG emissions for inland and municipal economy in Chongqing: factor dynamics and structure decomposition. Energy Procedia 104, 159–164. https://doi.org/10.1016/j.egypro.2016.12.028.

Hu, K., Yang, X., Zhong, J., Fei, F., Qi, J., 2017. Spatially explicit mapping of heat health risk utilizing environmental and socioeconomic data. Environ. Sci. Technol. 51, 1498–1507. https://doi.org/10.1021/acs.est.6b04355.

Ikram, M., Yan, Z., Liu, Y., Wu, D., 2015. Assessing the possible impacts of temperature change on air quality and public health in Beijing, 2008–2012. Nat. Hazards 84, 1–13. https://doi.org/10.1007/s11069-015-2061-7.

Jiao, P.P., Guo, Y.Z., 2014. Multiple features fusion based on PCA in liver CT image recognition. Appl. Mech. Mater. 484-485, 916–921. https://doi.org/10.4028/www.scientific.net/AMM.484-485.916.

Johnson, D.P., Wilson, J.S., Luber, G.C., 2009. Socioeconomic indicators of heat-related health risk supplemented with remotely sensed data. Int. J. Health Geogr. 8, 57. https://doi.org/10.1186/1476-072X-8-57.
Johnson, D.P., Stanforth, A., Lulla, V., Luber, G., 2012. Developing an applied extreme heat vulnerability index utilizing socioeconomic and environmental data. Appl. Geogr. 35, 23–31. https://doi.org/10.1016/j.apgeog.2012.04.006.
Kanasi, E., Ayilavarapu, S., Jones, J., 2016. The aging population: demographics and the biology of aging. Periodontology 72, 13–18. https://doi.org/10.1111/prd.12126.
Keller, R.C., 2013. Place matters: mortality, space, and urban form in the 2003 Paris Heat Wave Disaster. Fr. Hist. Stud. 36, 299–330. https://doi.org/10.1215/00161071-1960682.
Kosatsky, T., Henderson, S.B., Pollock, S.L., 2012. Shifts in mortality during a hot weather event in Vancouver, British Columbia: rapid assessment with case-only analysis. Am. J. Public Health 102, 2367–2371. https://doi.org/10.2105/AJPH.2012.300670.
Krstic, N., Yuchi, W., Ho, H.C., Walker, B.B., Knudby, A.J., Henderson, S.B., 2017. The Heat Exposure Integrated Deprivation Index (HEIDI): a data-driven approach to quantifying neighborhood risk during extreme hot weather. Environ. Int. 109, 42–52. https://doi.org/10.1016/j.envint.2017.09.011.
Lang, T., 2011. Advancing global health research through digital technology and sharing data. Science 331, 714–717. https://doi.org/10.1126/science.1199349.
Li, L.W., Zhang, J., 2015. Challenges to Successful Aging in Transitional China. Springer, Netherlands.
Li, B., Alistair, W., Cirendunzhu, Liu, Q., 2016. County-level heat vulnerability of urban and rural residents in Tibet, China. Environ. Health 15, 1–10. https://doi.org/10.1186/s12940-015-0081-0.
Li, Y., Li, C., Luo, S., He, J., Cheng, Y., Jin, Y., 2017. Impacts of extremely high temperature and heatwave on heatstroke in Chongqing, China. Environ. Sci. Pollut. Res. 24, 1–7. https://doi.org/10.1007/s11356-017-8457-z.
Li, J., Zhai, C., Yu, J., Liu, R., Li, Y., Zeng, L., Xie, S., 2018. Spatiotemporal variations of ambient volatile organic compounds and their sources in Chongqing, a mountainous megacity in China. Sci. Total Environ. 627, 1442–1452. https://doi.org/10.1016/j.scitotenv.2018.02.010.
Lissner, T.K., Holsten, A., Walther, C., Kropp, J.P., 2012. Towards sectoral and standardised vulnerability assessments: the example of heatwave impacts on human health. Clim. Chang. 112, 687–708. https://doi.org/10.1007/s10584-011-0231-5.
Liu, M., Xu, X., Sun, A.Y., Wang, K., Liu, W., Zhang, X., 2014. Is southwestern China experiencing more frequent precipitation extremes? Environ. Res. Lett. 9, 479–489. https://doi.org/10.1088/1748-9326/9/6/064002.
Loughnan, M.E., Tapper, N.J., Phan, T., Mcinnes, J.A., 2014. Can a spatial index of heat-related vulnerability predict emergency service demand in Australian capital cities? Int. J. Emerg. Serv. 3, 6–33. https://doi.org/10.1108/IJES-10-2012-0044.
Luis, I., Massimo, P., Francisco, D.L.B., 2016. A heat vulnerability index: spatial patterns of exposure, sensitivity and adaptive capacity for Santiago de Chile. PLoS One 11, e162464. https://doi.org/10.1371/journal.pone.0162464.
Lutz, W., Sanderson, W., Scherbov, S., 2008. The coming acceleration of global population ageing. Nature 451, 716–719. https://doi.org/10.1038/nature06516.
Ma, H., Shao, H., Song, J., 2014. Modeling the relative roles of the foehn wind and urban expansion in the 2002 Beijing heat wave and possible mitigation by high reflective roofs. Meteorog. Atmos. Phys. 123, 105–114. https://doi.org/10.1007/s00703-013-0289-x.
Ma, L., Wu, J., Li, W., Peng, J., Liu, H., 2014. Evaluating saturation correction methods for DMSP/OLS nighttime light data: a case study from China's cities. Remote Sens. 6, 9853–9872. https://doi.org/10.3390/rs6109853.
Ma, Y., Xu, W., Zhao, X., Li, Y., 2017. Modeling the hourly distribution of population at a high spatiotemporal resolution using subway smart card data: a case study in the central area of Beijing. Int. J. Geo-Inf. 6, 128. https://doi.org/10.3390/ijgi6050128.
Macintyre, H.L., Heaviside, C., Taylor, J., Picetti, R., Symonds, P., Cai, X.M., Vardoulakis, S., 2017. Assessing urban population vulnerability and environmental risks across an urban area during heatwaves - implications for health protection. Sci. Total Environ. 610-611, 678. https://doi.org/10.1016/j.scitotenv.2017.08.062.
Macnee, R.G.D., Tokai, A., 2016. Heat wave vulnerability and exposure mapping for Osaka City, Japan. Environ. Syst. Decis. 36, 368–376. https://doi.org/10.1007/s10669-016-9607-4.
Meehl, G.A., Tebaldi, C., 2004. More intense, more frequent, and longer lasting heat waves in the 21st century. Science 305, 994–997. https://doi.org/10.1126/science.1098704.
Mees, H.L.P., Driessen, P.P.J., Runhaar, H.A.C., 2014. "Cool" governance of a "hot" climate issue: public and private responsibilities for the protection of vulnerable citizens against extreme heat. Reg. Environ. Chang. 15, 1–15. https://doi.org/10.1007/s10113-014-0681-1.
Merbitz, H., Buttstädt, M., Michael, S., Dott, W., Schneider, C., 2012. GIS-based identification of spatial variables enhancing heat and poor air quality in urban areas. Appl. Geogr. 33, 94–106. https://doi.org/10.1016/j.apgeog.2011.06.008.
Mora, C., Dousset, B., Caldwell, I.R., Powell, F.E., Geronimo, R.C., Bielecki, C.R., Counsell, C.W.W., Dietrich, B.S., Johnston, E.T., Louis, L.V., 2017. Global risk of deadly heat. Nat. Clim. Chang. 7, 501–507. https://doi.org/10.1038/nclimate3322.
Morabito, M., Crisci, A., Gioli, B., Gualtieri, G., Toscano, P., Stefano, V.D., Orlandini, S., Gensini, G.F., 2015. Urban-hazard risk analysis: mapping of heat-related risks in the elderly in major Italian cities. PLoS One 10, e127277. https://doi.org/10.1371/journal.pone.0127277.
NASA, 2010a. MODIS Land surface temperature products. https://ladsweb.modaps.eosdis.nasa.gov/search/, Accessed date: June 2019.
NASA, 2010b. Enhanced Vegetation Index (EVI) data. https://ladsweb.modaps.eosdis.nasa.gov/search/, Accessed date: June 2019.
NASA, 2011. ASTER GDEM. https://search.earthdata.nasa.gov/search/granules?p=C197265171-LPDAAC_ECS&q=gdem&ok=gdem, Accessed date: June 2019.
Neuman, M., Kawachi, I., Gortmaker, S., Subramanian, S.V., 2013. Urban-rural differences in BMI in low- and middle-income countries: the role of socioeconomic status. Am. J. Clin. Nutr. 97, 428–436. https://doi.org/10.3945/ajcn.112.045997.
Nie, J.B., 2016. Erosion of eldercare in China: a socio-ethical inquiry in aging, elderly suicide and the Government's responsibilities in the context of the one-child policy. Ageing Int. 41, 1–16. https://doi.org/10.1007/s12126-016-9261-7.
NOAA, 2010. DMSP/OLS, NTL. https://www.ngdc.noaa.gov/eog/dmsp/downloadV4composites.html, Accessed date: June 2019.
Obradovich, N., Migliorini, R., Mednick, S.C., Fowler, J.H., 2017. Nighttime temperature and human sleep loss in a changing climate. Sci. Adv. 3, e1601555. https://doi.org/10.1126/sciadv.1601555.
Palmer, J., Bennetts, H., Pullen, S., Zuo, J., Ma, T., Chileshe, N., 2014. The effect of dwelling occupants on energy consumption: the case of heat waves in Australia. Archit. Eng. Des. Manag. 10, 40–59. https://doi.org/10.1080/17452007.2013.837247.
Patel, N.N., Angiuli, E., Gamba, P., Gaughan, A., Lisini, G., Stevens, F.R., Tatem, A.J., Trianni, G., 2015. Multitemporal settlement and population mapping from Landsat using Google Earth Engine. Int. J. Appl. Earth Obs. Geoinf. 35, 199–208. https://doi.org/10.1016/j.jag.2014.09.005.
Patel, N.N., Stevens, F.R., Huang, Z., Gaughan, A.E., Elyazar, I., Tatem, A.J., 2017. Improving large area population mapping using Geotweet densities. Trans. GIS 21, 317–331. https://doi.org/10.1111/tgis.12214.
Peel, M.C., Finlayson, B.L., Mcmahon, T.A., 2007. Updated world map of the Köppen-Geiger climate classification. Hydrol. Earth Syst. Sci., 1633–1644 https://doi.org/10.5194/hess-11-1633-2007.
Pincetl, S., Chester, M., Eisenman, D., 2016. Urban heat stress vulnerability in the U.S. southwest: the role of sociotechnical systems. Sustainability 8, 842. https://doi.org/10.3390/su8090842.
Priyanka, Chakravarty, A., 2015. Correlates of body mass index (BMI) with their socioeconomic status of urban and rural adults of Varanasi district. Asian J. Home Sci. 10, 108–115. https://doi.org/10.15740/HAS/AJHS/10.1/108-115.
Raza, M., Azhar, S., Murtaza, G., Syed, A., Khan, A., Saleem, F., Raza, M., Azhar, S., Murtaza, G., Syed, A., 2017. Immunization status of children in Abbottabad, Pakistan: a cross-sectional study. 7, 177–183. https://doi.org/10.25258/ijddt.v7i03.9561.
Reid, C.E., Mann, J.K., Alfasso, R., English, P.B., King, G.C., Lincoln, R.A., Margolis, H.G., Dan, J.R., Sabato, J.E., West, N.L., 2012. Evaluation of a heat vulnerability index on abnormally hot days: an environmental public health tracking study. Environ. Health Perspect. 120, 715–720. https://doi.org/10.1289/ehp.1103766.
Romero-Lankao, P., Qin, H., Dickinson, K., 2012. Urban vulnerability to temperature-related hazards: a meta-analysis and meta-knowledge approach. Glob. Environ. Chang. 22, 670–683. https://doi.org/10.1016/j.gloenvcha.2012.04.002.
Rosina, K.T.N., Hurbā Nek, P., Cebecauer, M., 2016. Using OpenStreetMap to improve population grids in Europe. Am. Cartogr. 44, 139–151. https://doi.org/10.1080/15230406.2016.1192487.
Sampson, N.R., Gronlund, C.J., Buxton, M.A., Catalano, L., White-Newsome, J.L., Conlon, K.C., O'Neill, M.S., Mccormick, S., Parker, E.A., 2013. Staying cool in a changing climate: reaching vulnerable populations during heat events. Glob. Environ. Chang. 23, 475–484. https://doi.org/10.1016/j.gloenvcha.2012.12.011.
Savory, D.J., Andradepacheco, R., Gething, P.W., Midekisa, A., Bennett, A., Sturrock, H.J.W., 2017. Intercalibration and Gaussian process modeling of nighttime lights imagery for measuring urbanization trends in Africa 2000–2013. Remote Sens. 9, 713. https://doi.org/10.3390/rs9070713.
Schuurman, N., Bell, N., Dunn, J.R., Oliver, L., 2007. Deprivation indices, population health and geography: an evaluation of the spatial effectiveness of indices at multiple scales. J. Urban Health 84, 591–603. https://doi.org/10.1007/s11524-007-9193-3.
Shaposhnikov, D., Revich, B., Bellander, T., Bedada, G.B., Bottai, M., Kharkova, T., Kvasha, E., Lezina, E., Lind, T., Semutnikova, E., 2014. Mortality related to air pollution with the Moscow heat wave and wildfire of 2010. Epidemiology 25, 359–364. https://doi.org/10.1097/EDE.0000000000000090.
Sheridan, S.C., Dolney, T.J., 2003. Heat, mortality, and level of urbanization: measuring vulnerability across Ohio, USA. Clim. Res. 24, 255–265. https://doi.org/10.3354/cr024255.
Son, J.Y., Lee, J.T., Anderson, G.B., Bell, M.L., 2012. The impact of heat waves on mortality in seven major cities in Korea. Environ. Health Perspect. 120, 566–571. https://doi.org/10.1289/ehp.1103759.
Song, G., Yu, M., Liu, S., Zhang, S., 2015. A dynamic model for population mapping: a methodology integrating a Monte Carlo simulation with vegetation-adjusted nighttime light images. Int. J. Remote Sens. 36, 4055–4068. https://doi.org/10.1080/01431161.2015.1073862.
Speirs, J.C., Steinhoff, D.F., Mcgowan, H.A., Bromwich, D.H., Monaghan, A.J., 2010. Foehn winds in the McMurdo dry valleys, Antarctica: the origin of extreme warming events. J. Clim. 23, 3577–3598. https://doi.org/10.1175/2010JCLI3382.1.
Tan, M., Li, X., Li, S., Xin, L., Wang, X., Li, Q., Li, W., Li, Y., Xiang, W., 2018. Modeling population density based on nighttime light images and land use data in China. Appl. Geogr. 90, 239–247. https://doi.org/10.1016/j.apgeog.2017.12.012.
Tao, L., Yan, J.X., Yong, H.Z., Yan, Q.H., Xiu, L.S., Hui, Y.X., Yuan, L., Rutherford, S., Chu, C., Hua, L.L., 2013. Associations between risk perception, spontaneous adaptation behavior to heat waves and heatstroke in Guangdong province, China. BMC Public Health 13, 913. https://doi.org/10.1186/1471-2458-13-913.
Tapia, C., Abajo, B., Feliu, E., Mendizabal, M., Martinez, J.A., Fernández, J.G., Laburu, T., Lejarazu, A., 2017. Profiling urban vulnerabilities to climate change: an indicator-based vulnerability assessment for European cities. Ecol. Indic. 78, 142–155. https://doi.org/10.1016/j.ecolind.2017.02.040.
Tenerelli, P., Gallego, J.F., Ehrlich, D., 2015. Population density modelling in support of disaster risk assessment. Int. J. Disaster Risk Reduct. 13, 334–341. https://doi.org/10.1016/j.ijdrr.2015.07.015.

Tomlinson, C.J., Chapman, L., Thornes, J.E., Baker, C.J., 2011. Including the urban heat island in spatial heat health risk assessment strategies: a case study for Birmingham, UK. Int. J. Health Geogr. 10, 1–14. https://doi.org/10.1186/1476-072X-10-42.

Tomusange, I., Yoon, A., Mukasa, N., 2017. The data sharing practices and challenges in Uganda. Proc. Assoc. Inf. Sci. Technol. 54, 814–815. https://doi.org/10.1002/pra2.2017.14505401168.

Unal, Y.S., Tan, E., Mentes, S.S., 2013. Summer heat waves over western Turkey between 1965 and 2006. Theor. Appl. Climatol. 112, 339–350. https://doi.org/10.1007/s00704-012-0704-0.

Urban, A., Hanzlíková, H., Kyselý, J., Plavcová, E., 2017. Impacts of the 2015 heat waves on mortality in the Czech Republic–a comparison with previous heat waves. Int. J. Environ. Res. Public Health 14, 1562. https://doi.org/10.3390/ijerph14121562.

USGS, 2012. Global surface water. https://landcover.usgs.gov/glc/WaterDescriptionAndDownloads.php, Accessed date: June 2019.

Vandentorren, S., Bretin, P., Zeghnoun, A., Mandereaubruno, L., Croisier, A., Cochet, C., Ribéron, J., Siberan, I., Declercq, B., Ledrans, M., 2006. August 2003 heat wave in France: risk factors for death of elderly people living at home. Eur. J. Pub. Health 16, 583–591. https://doi.org/10.1093/eurpub/ckl063.

Voelkel, J., Hellman, D., Sakuma, R., Shandas, V., 2018. Assessing vulnerability to urban heat: a study of disproportionate heat exposure and access to refuge by socio-demographic status in Portland, Oregon. Int. J. Environ. Res. Public Health 15, 640. https://doi.org/10.3390/ijerph15040640.

Wang, J., Feng, J., Yan, Z., Hu, Y., Jia, G., 2012. Nested high-resolution modeling of the impact of urbanization on regional climate in three vast urban agglomerations in China. J. Geophys. Res. Atmos. 117, 21103. https://doi.org/10.1029/2012JD018226.

Weber, S., Sadoff, N., Zell, E., Sherbinin, A.D., 2015. Policy-relevant indicators for mapping the vulnerability of urban populations to extreme heat events: a case study of Philadelphia. Appl. Geogr. 63, 231–243. https://doi.org/10.1016/j.apgeog.2015.07.006.

WHO, 2015. World report on ageing and health 2015. http://www.who.int/ageing/publications/world-report-2015/en/, Accessed date: September 2019.

WHO, 2018. Ageing and health. http://www.who.int/news-room/fact-sheets/detail/ageing-and-health, Accessed date: September 2019.

Willers, S.M., Jonker, M.F., Klok, L., Keuken, M.P., Odink, J., Van, D.E.S., Sabel, C.E., Mackenbach, J.P., Burdorf, A., 2016. High resolution exposure modelling of heat and air pollution and the impact on mortality. Environ. Int. 89-90, 102. https://doi.org/10.1016/j.envint.2016.01.013.

Wolf, T., Mcgregor, G., 2013. The development of a heat wave vulnerability index for London, United Kingdom. Weather Clim. Extrem. 1, 59–68. https://doi.org/10.1016/j.wace.2013.07.004.

Wolf, T., Mcgregor, G., Analitis, A., 2014. Performance assessment of a heat wave vulnerability index for Greater London, United Kingdom. Weather Clim. Soc. 6, 32–46. https://doi.org/10.1175/WCAS-D-13-00014.1.

Wolf, T., Chuang, W.C., McGregor, G., 2015. On the science-policy bridge: do spatial heat vulnerability assessment studies influence policy? Int. J. Environ. Res. Public Health 12, 13321–13349. https://doi.org/10.3390/ijerph121013321.

Wu, P.C., Lin, C.Y., Lung, S.C., Guo, H.R., Chou, C.H., Su, H.J., 2011. Cardiovascular mortality during heat and cold events: determinants of regional vulnerability in Taiwan. Occup. Environ. Med. 68, 525–530. https://doi.org/10.1136/oem.2010.056168.

Xu, Z., Sheffield, P.E., Su, H., Wang, X., Bi, Y., Tong, S., 2014. The impact of heat waves on children's health: a systematic review. Int. J. Biometeorol. 58, 239. https://doi.org/10.1007/s00484-013-0655-x.

Yang, X.C., Yue, W.Z., Gao, D.W., 2013. Spatial improvement of human population distribution based on multi-sensor remote-sensing data: an input for exposure assessment. Int. J. Remote Sens. 34, 5569–5583. https://doi.org/10.1080/01431161.2013.792970.

Zhang, J.F., Deng, W., 2010. Industrial structure change and its eco-environmental influence since the establishment of municipality in Chongqing, China. Procedia Environ. Sci. 2, 517–526. https://doi.org/10.1016/j.proenv.2010.10.056.

Zhang, Z., Cheng, Y., Liu, N.C., 2014. Comparison of the effect of mean-based method and z-score for field normalization of citations at the level of Web of Science subject categories. Scientometrics 101, 1679–1693. https://doi.org/10.1007/s11192-014-1294-7.

Zhang, W., Zhu, Y., Jiang, J., 2016. Effect of the urbanization of wetlands on microclimate: a case study of Xixi Wetland, Hangzhou, China. Sustainability 8, 885. https://doi.org/10.3390/su8090885.

Zhou, Q., Ma, Z., Liang, T., Xiang, J., Cheng, Y., Han, L., 2010. Researched on urban expansion and climate responses of Chongqing in the past 30 years. Paper Presented at: International Conference on Environmental Science and Information Application Technology https://doi.org/10.1109/ESIAT.2010.5567257.

Zhu, Z., Bi, J., Pan, Y., Ganguly, S., Anav, A., Xu, L., Samanta, A., Piao, S., Nemani, R.R., Myneni, R.B., 2013. Global data sets of vegetation leaf area index (LAI)3g and fraction of photosynthetically active radiation (FPAR)3g derived from global inventory modeling and mapping studies (GIMMS) normalized difference vegetation index (NDVI3g) for the period 1981 to 20. Remote Sens. 5, 927–948. https://doi.org/10.3390/rs5020927.

Zhu, Q., Liu, T., Lin, H., Xiao, J., Luo, Y., Zeng, W., Zeng, S., Wei, Y., Chu, C., Baum, S., 2014. The spatial distribution of health vulnerability to heat waves in Guangdong Province, China. Glob. Health Action 7, 25051. https://doi.org/10.3402/gha.v7.25051.

Zografos, C., Anguelovski, I., Grigorova, M., 2016. When exposure to climate change is not enough: exploring heatwave adaptive capacity of a multi-ethnic, low-income urban community in Australia. Urban Clim. 17, 248–265. https://doi.org/10.1016/j.uclim.2016.06.003.